Publisher source acknowledgment: https://doi.org/10.1021/acs.jmedchem.2c02093 (final version)

A New Antidiabetic Agent Showing Short- and Long-Term Effects Due To Peroxisome Proliferator-Activated Receptor Alpha/Gamma Dual Agonism and Mitochondrial Pyruvate Carrier Inhibition

Antonio Laghezza,[1] Carmen Cerchia,[2] Massimo Genovese,[3] Rosalba Leuci,[1] Erica Pranzini,[3] Alice Santi,[3] Leonardo Brunetti,[1] Luca Piemontese,[1] Paolo Tortorella,[1] Abanish Biswas,[4] Ravi Pratap Singh,[4] Suhas Tambe,[5] Sudeep Ca,[6] Ashok Kumar Pattnaik,[4] Venkatesan Jayaprakash,[4] Paolo Paoli,[3] Antonio Lavecchia,[2*] Fulvio Loiodice[1*]

[1] *Dipartimento Farmacia-Scienze del Farmaco, Università degli Studi di Bari "Aldo Moro", via Orabona 4, 70125 Bari, Italy*

[2] *Dipartimento di Farmacia, "Drug Discovery" Laboratory, Università degli Studi di Napoli "Federico II", via D. Montesano 49, 80131 Napoli, Italy*

[3]*Dipartimento di Scienze Biomediche Sperimentali e Cliniche, Sezione di Scienze Biochimiche, Università degli Studi di Firenze, Viale Morgagni 50, 50134, Firenze, Italy*

[4]*Department of Pharmaceutical Sciences & Technology, Birla Institute of Technology, Mesra, Ranchi, Jharkhand 835215 India*

[5]*Adgyl Lifescience Private Ltd., Bengaluru 560058 India*

[6]*Bioanalytical Section, Eurofins Advinus Biopharma Services India Pvt Ltd., Bengaluru 560058 India*

ABSTRACT

A new series of analogs or derivatives of the previously reported PPARα/γ dual agonist LT175 allowed the identification of ligand **10**, which was able to potently activate both PPARα and -γ subtypes as full and partial agonist, respectively. Docking studies were performed to provide a molecular explanation for this different behavior on the two different targets. In vivo experiments showed that this compound induced a significant reduction of blood glucose and lipid levels in a streptozotocin-induced diabetic mice model displaying no toxic effects on bone, kidney, and liver. By examining in depth the antihyperglycemic activity of **10**, we found out that it produced a slight but significant inhibition of mitochondrial pyruvate carrier acting also through insulin-independent mechanisms. This is the first example of PPARα/γ dual agonist reported to show this inhibitory effect representing, therefore, the potential lead of a new class of drugs for treatment of dyslipidemic type 2 diabetes.

INTRODUCTION

Type 2 diabetes mellitus (T2DM) and dyslipidemia are established risk factors documented to play a pivotal role in cardiovascular diseases (CVDs), which have emerged as the leading cause of morbidity and mortality worldwide.[1,2] Diabetic dyslipidemia is characterized by insulin resistance, high levels of triglycerides and small dense low-density lipoproteins (LDL), and low levels of high-density lipoproteins (HDL).[3] Despite the widespread use of statins to lower cholesterol and reduce cardiovascular morbidity and mortality, patients with dyslipidemia remain at a high residual risk of developing CVDs and this risk is further increased in T2DM patients.[4,5]

Peroxisome proliferator-activated receptors (PPARs) are ligand-activated transcription factors that play a key role in the regulation of a large number of genes whose products are directly or indirectly involved in glucose homeostasis and lipid metabolism. For this reason, they have been considered suitable targets for the treatment of metabolic disorders.[6] The PPARs family comprises three different subtypes: α, β/δ and γ, whose expression and actions differ according to subtype, organ and tissue cell type.[6] PPARα is expressed in tissues with a high rate of fatty acid oxidation, such as skeletal muscle, liver, heart, kidney and brown adipose tissue, and modulates lipid metabolism and inflammation.[7] PPARγ is mainly expressed in adipose tissue, where it induces lipogenesis and fat storage, and in skeletal muscle, where it improves insulin sensitivity.[8] PPARδ, the less understood PPAR subtype, is more ubiquitously expressed; it is involved in metabolic disorders, inflammation, and angiogenesis.[9]

PPARα or PPARγ agonist drugs, such as fibrates or thiazolidinediones (TZDs), have been widely employed for lipid and glycemic control.[10] Safety-related issues with fibrates[11] prompted the development of PPARα agonists with improved clinical efficacy, such as pemafibrate, endowed with superior benefit-risk balance compared to conventional fibrates.[12] The use of TZDs like rosiglitazone or pioglitazone has been limited, or they have been withdrawn from the market in the

United States, Europe and other countries,[13] due to unwanted adverse effects, such as fluid retention, congestive heart failure (CHF) and adipogenic weight gain.[10] To overcome these issues, research efforts have been ultimately directed towards the design of new molecules beneficially altering carbohydrate and lipid metabolism in a coordinated manner. In recent years, PPARα/γ dual agonists have been considered as promising new treatment options for the development of hypolipidemic and antidiabetic drugs. PPARα agonists improve lipid profile, whereas PPARγ agonist action improves glucose profile in patients with diabetic dyslipidemia.[14-17] Recently, one such agent, saroglitazar, has been approved in India for the treatment of diabetic dyslipidemia and hypertriglyceridemia with type 2 diabetes not controlled by statin therapy.[5] Saroglitazar is predominantly a PPARα agonist, with modest PPARγ agonist actions. This is in contrast to previously developed dual PPARα/γ agonists, which had either predominantly PPARγ agonistic activity or similar agonistic activity on both PPARα and PPARγ receptors. In particular, an appropriate modulation of PPARγ activity appears the key challenge for the development of a dual agonist able to uncouple the adverse effects of the ligand from therapeutic effects.

In our previous studies, we identified the lead compound LT175 (Figure 1), a dual PPARα/γ ligand with a partial agonism profile toward the γ subtype.[18] The X-ray structure of the complex with PPARγ showed that this compound interacts with the receptor in a newly identified hydrophobic region called “diphenyl pocket” inducing a conformation of the ligand binding domain (LBD) less favorable to the recruitment of coactivators required for full activation of PPARγ. This new interaction influences the expression of PPARγ target genes, leading to an improved therapeutic profile compared with rosiglitazone. In fact, LT175 showed potent insulin-sensitizing effects with reduced adipogenic properties.[19] At the same time, this ligand, by activating PPARα in the liver, triggers triglyceride and fatty acid catabolism and provides additional beneficial effects because of lipid clearing. These features make LT175 a promising scaffold molecule to design new ligands with better metabolic profiles on both glucose and lipid parameters.[19] With this aim, in the past we

have prepared two new series of LT175 analogs in which the biological effects resulting from modifications of the diphenyl system have been evaluated.[20,21] In the present work, instead, we decided to focus our attention on the 2-oxy-3-phenyl propanoic acid moiety by bringing about a series of chemical modifications, which led to the synthesis of compounds **1-15** reported in Figure 1. Analogs **1-10** were prepared as racemates, whereas compounds **11-15**, being derivatives of LT175, were obtained as *S* isomers. Noteworthy, we identified some new ligands showing an interesting PPARα/γ dual activity, whereas three of them behaved as antagonists.

Compound **10** turned out to be the ligand with the most interesting pharmacological profile able to potently activate both PPARα and -γ subtypes as full and partial agonist, respectively. Docking studies were performed to provide a molecular explanation for this different behavior and gain insight into the main interactions at the binding sites of the two different targets.

On the basis of structural and pharmacological similarity with LT175, we decided to evaluate the effects of **10** in a streptozotocin (STZ)-induced diabetic mice model. Interestingly, this compound showed a significant reduction of blood glucose and lipid levels displaying, at the same time, no toxic effects on bone, kidney, and liver. Based upon these results, with the aim to examine in depth the antihyperglycemic activity of **10**, we decided to verify if these effects could be explained only by transcriptional events following PPAR activation or other mechanisms occurred. We studied different targets and found out that a slight but significant inhibition of mitochondrial pyruvate carrier could be responsible, at least in part, of the increased glucose uptake we observed in C2C12 muscle cell line. These results confirm that **10** also acts through insulin-independent mechanisms, which need other experiments to be elucidated, but, at the same time, allow to claim that this compound may represent a very promising candidate as the lead of a new class of drugs for treatment of dyslipidemic type 2 diabetes.

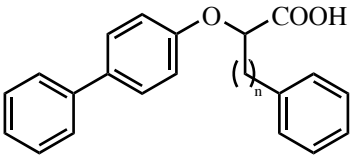

LT175 n = 1 (S isomer)

1. n = 0

2. n = 2

3. n = 3

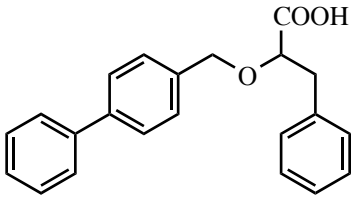

4

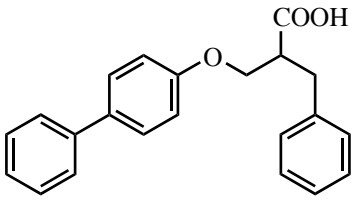

5

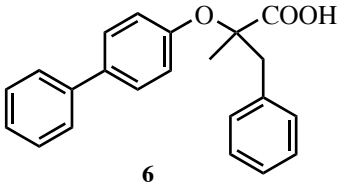

6

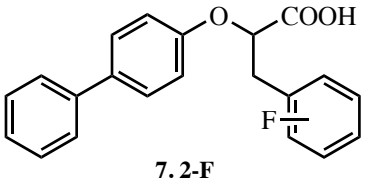

7. 2-F

8. 4-F

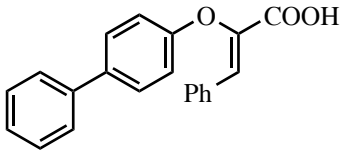

9

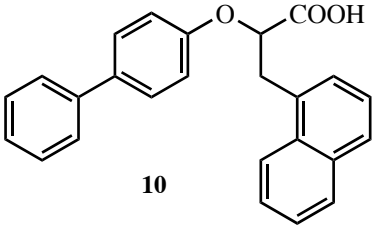

10

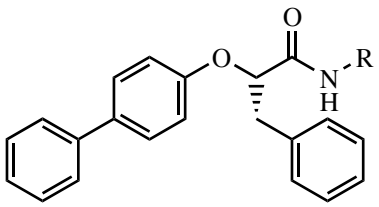

11. R = SO_2CH_3

12. R = SO_2 *p*-tolyl

15. R = Ph

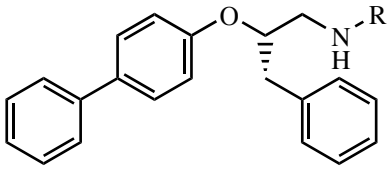

13. R = SO_2CH_3

14. R = SO_2Ph

Figure 1. Structure of the molecules object of the present study.

Chemistry. The preparation of racemates **2**, **3**, **7**, **8** and **10** started from intermediate **16** obtained by condensation between diethyl bromomalonate and 4-phenylphenate in refluxing acetone (Scheme 1).[22] This intermediate was reacted with the appropriate arylalkyl bromides in the presence of 95% NaH powder affording diethyl esters **2a**, **3a**, **7a**, **8a**, and **10a** whose basic hydrolysis followed from thermal decarboxylation at 160 °C led to the target compounds.[23]

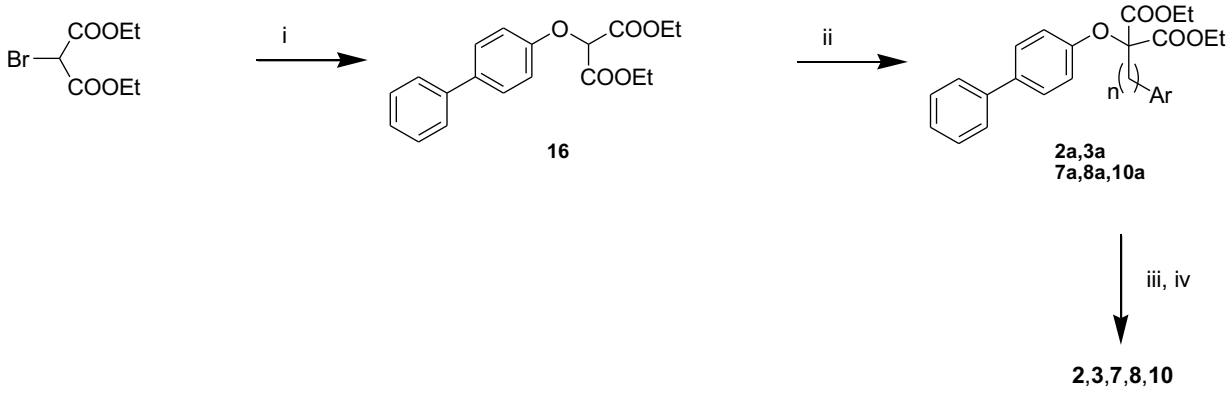

Scheme 1. (i) Na, abs EtOH, acetone, 4-phenylphenol, reflux, overnight; (ii) arylalkyl bromide, 95% NaH powder, anhydrous DMF, N_2, 80 °C, overnight; (iii) 1M NaOH, abs EtOH, reflux, overnight; (iv) decarboxylation at 160 °C, 1 h.

Scheme 2 describes the synthesis of compounds **1** and **4**. Methyl 2-bromo-2-phenylacetate **1a** or ethyl 2-hydroxy-3-phenylpropanoate **4a** were converted to **1b** or **4b** by condensation with 4-phenylphenol or 4-bromobenzyl bromide, respectively. Compound **1** was obtained by basic hydrolysis of **1b**, whereas **4b** was reacted with phenyl boronic acid by Suzuki conditions obtaining the intermediate **4c** whose basic hydrolysis led to acid **4**.

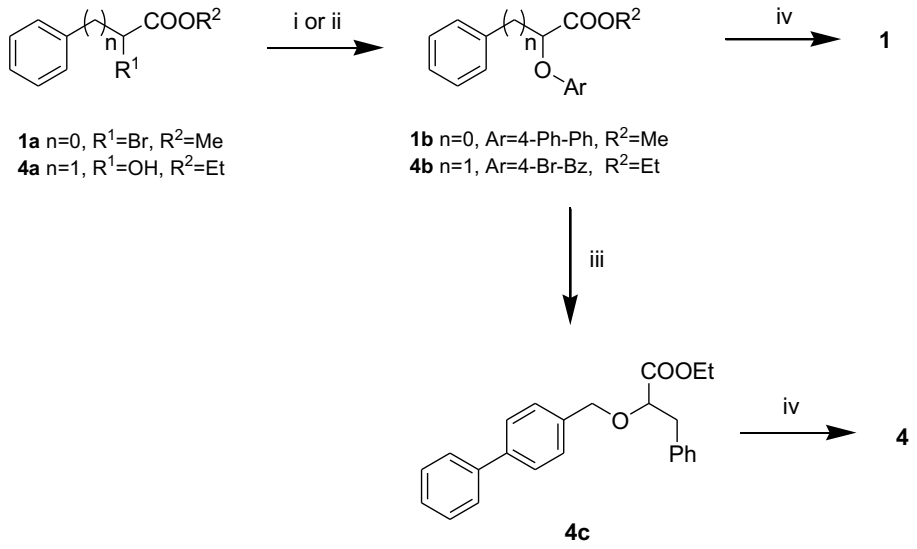

Scheme 2. (i) Na, abs EtOH, 4-phenylphenol, reflux, overnight; (ii) 4-bromobenzyl bromide, 95% NaH powder, anhydrous THF, N_2, 0°C→reflux, overnight; (iii) Phenyl boronic acid, Cs_2CO_3, $Pd[(C_6H_5)_3P]_4$, anhydrous toluene, N_2, H_2O, reflux, 24 h. (vi) 1M NaOH, THF, rt, 5 h.

Synthesis of compound **5** is reported in Scheme 3 and started from diethyl malonate which was condensed with benzyl bromide in the presence of NaH to give **5a**. This intermediate was reduced with $LiAlH_4$ leading to **5b** whose condensation with 4-phenylphenol under Mitsunobu conditions in the presence of triphenylphosphine and diisopropyl azodicarboxylate (DIAD) afforded **5c**, which was finally converted to the target acid **5** by oxidation with $NaIO_4$ using RuO_2 as a catalyst.[24]

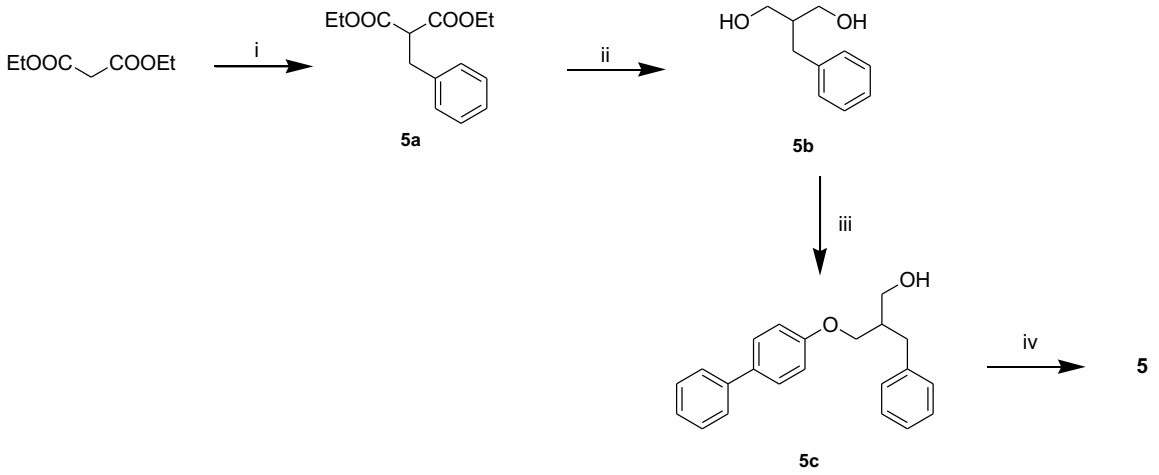

Scheme 3. (i) benzyl bromide, 95% NaH powder, anhydrous DMF, N_2, 0°C→rt, overnight; (ii) $LiAlH_4$, anhydrous THF, N_2, 0°C→rt, 3h; (iii) 4-phenylphenol, PPh_3, DIAD, anhydrous toluene, N_2, 0°C→rt, overnight; (iv) $NaIO_4$ (aq. sol. 10% w/v), $RuO_2 \cdot H_2O$, rt, 24h.

Compounds **6** was prepared starting from phenyl acetone and 4-phenylphenol (Scheme 4) according to the Bargellini conditions, using chloroform as a reagent in the presence of NaOH solution as a base.[25]

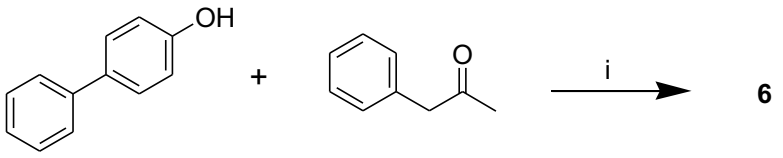

Scheme 4. (i) NaOH, $CHCl_3$, rt, overnight.

Scheme 5 describes the synthesis of compound **9** which started from the preparation of **9a** from 4-phenylphenol and ethyl bromoacetate. The condensation of **9a** with benzaldehyde in the presence of

lithium diisopropylamide (LDA) and subsequent treatment with benzenesulfonyl chloride gave the sulfonic intermediate **9b.** The reaction with refluxing triethylamine followed from basic hydrolysis led to final compound **9**, obtained only as *Z*-isomer.[26]

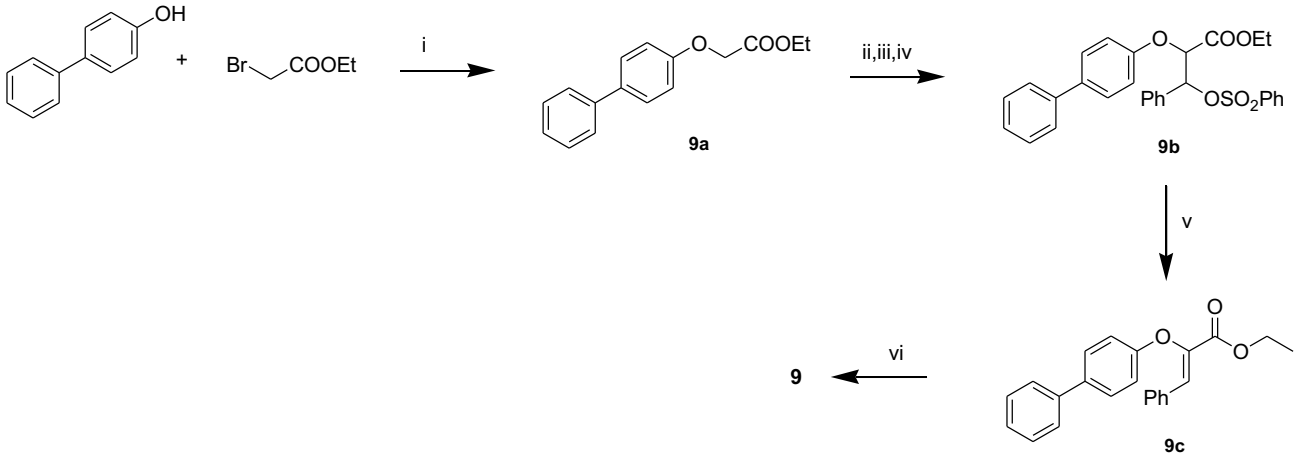

Scheme 5. i) abs EtOH, Na, reflux, 24 h; ii) LDA, anhydrous THF, N_2, -78°C, 20 min; iii) PhCHO, -30 °C; iv) $PhSOCl_2$, rt, overnight; v) triethylamine, reflux, 3h; vi) 3M NaOH, abs EtOH, reflux, 2h.

The synthesis of compounds **11-15** is reported in Scheme 6. Acylsulfonamides **11** and **12** were prepared by condensation of LT175 with the suitable commercial sulfonamide in the presence of dimethylaminopyridine (DMAP) and *N*-(3-dimethylaminopropyl)-*N'*-ethylcarbodiimide (EDCl). For the synthesis of amide **15**, the acyl chloride of LT175 was reacted with aniline. Sulfonamides **13** and **14** were also prepared starting from the acyl chloride of LT175, which was treated with 30% NH_4OH to give amide **17**; the reduction by 1M borane in THF afforded **18** whose condensation with the suitable sulfonyl chloride in the presence of triethylamine led to the final compounds **13** and **14**.

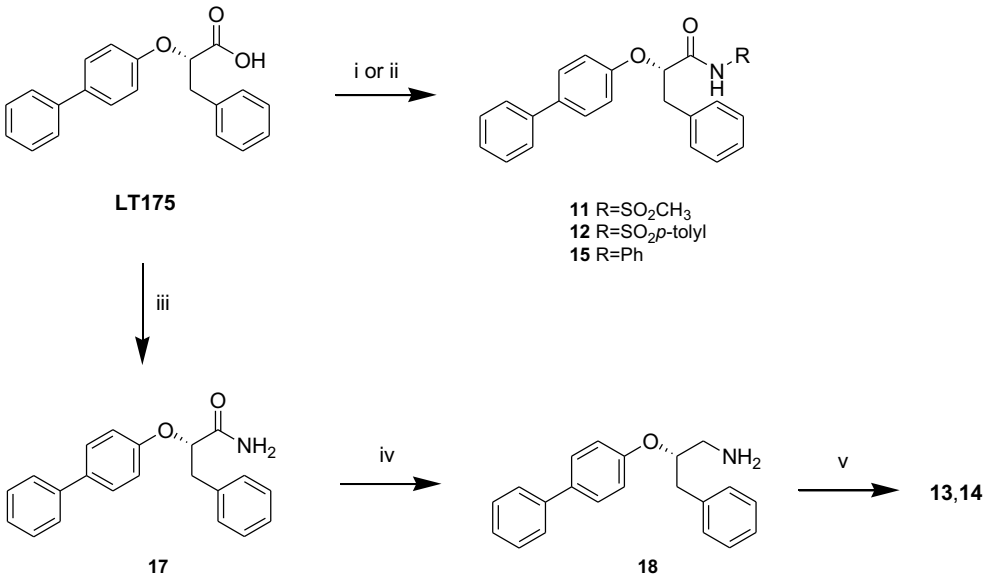

Scheme 6. (i) substituted sulfonamide, DMAP, EDCl, CH_2Cl_2, 0 °C → rt, 46 h; (ii) $SOCl_2$, reflux, 5 h; aniline, anhydrous THF, N_2, 0 °C→ reflux 2h→rt 24 h; (iii) $SOCl_2$, reflux, 2 h; NH_4OH 30%, THF, N_2, 0 °C→ rt 2h; (iv) 1M BH_3·THF, anhydrous THF, N_2, reflux, 3h; (v) substituted sulfonyl chloride, triethylamine, anhydrous THF, N_2, 0 °C, 2h.

RESULTS AND DISCUSSION

PPAR Activity. Compounds **1**−**15** were evaluated in vitro for their agonist activity toward the human PPARα (hPPARα) and PPARγ (hPPARγ) subtypes by employing GAL4-PPAR transactivation assay. For this purpose, GAL4-PPAR chimeric receptors were expressed in transiently transfected HepG2 cells according to a previously reported procedure.[27] In particular, the results obtained were compared with corresponding data for Wy-14,643 and rosiglitazone used as reference compounds in the PPARα and PPARγ transactivation assays, respectively. Maximum obtained fold induction with the reference agonist was defined as 100%. The activity of **1**−**15** was also compared with the lead compound LT175 (Table 1).

Table 1. Biological activities of novel analogues of LT175 on PPARs.

	PPARα		PPARγ	
Cpd	Emax %[a]	EC_{50} (μM)	Emax %[a]	EC_{50} (μM)
LT175	116±4	0.23±0.02	62±7	0.48±0.06
1	46±1	1.24±0.16	12±1	12.1±1.5
2	77±14	1.38±0.02	40±1	1.75±0.78
3	85±8	0.56±0.07	65±5	1.59±0.08
4	43±18	0.63±0.15	49±7	2.36±0.06
5	i	-	40±6	3.3±1.2
6	129±9	0.204±0.019	91±9	0.88±0.07
7	72±5	1.16±0.28	67±3	1.4±0.3
8	88±6	1.08±0.24	71±4	1.19±0.3
9	63±1	1.78±0.01	44±2	2.04±0.11
10	97±1	0.95±0.30	60±1	0.91±0.27
11	58±6	1.49±0.09	9±1	7.7±2.2
12	(antagonist)	(IC_{50}) 3.75±0.38	(antagonist)	(IC_{50}) 5.9±0.1
13	(antagonist)	(IC_{50}) 7.8±0.8	(antagonist)	(IC_{50}) 14.8±3.5
14	(antagonist)	(IC_{50}) 15.0±0.8	i	-
15	i	-	i	-
Wy-14,643	1.56±0.30	100±10	-	-
Rosiglitazone	-	-	0.039±0.003	100±9

[a]Efficacy values were calculated as a percentage of the maximum obtained fold induction with the reference compounds; i = inactive at tested concentration.

The first chemical modification consisted in the change of the length of the phenyl propanoic acid moiety. The removal of the benzylic methylene (compound **1**) was detrimental for potency and efficacy on both receptor subtypes, especially PPARγ, whereas the lengthening of the chain led to the more flexible and active compounds **2** and **3** with the phenyl pentanoic acid analog **3** showing only less potency than LT175 on PPARγ. The introduction of a methylene between the diphenylic system and the oxygen (compound **4**) significantly reduced potency and efficacy on both receptors. The same effect was obtained on PPARγ by introduction of a methylene between the phenolic oxygen and the carboxylic group (compound **5**), whereas the activity of this compound on PPARα was completely abolished. The introduction of a methyl on the stereogenic center allowed to obtain compound **6** with a sterically hindered quaternary carbon atom whose presence in bioactive small molecules could promote an element of conformational restriction that is shown to impart increased potency and metabolic stability.[28] In fact, this compound turned out to be a dual PPARα/γ full agonist with sub-micromolar potency on both receptors and also behaving as PPARα "superagonist" (Emax = 129 ± 9). These effects were comparable to those obtained with LT175 even though **6** is a racemate; if one considers that PPARs show a high degree of stereoselectivity towards several classes of drugs, in particular those characterized by the presence of a stereogenic center close to a carboxylic function, it is reasonable to suppose even higher potency and efficacy for the eutomer of this compound.

With the aim to investigate the possibility to fine-tune the activity of LT175, we synthesized two new compounds in which a fluorine atom was introduced in ortho (**7**) or para position (**8**) of the benzylic ring. Fluorine generally has a profound effect on the physical and/or biological properties of the target molecule. Its introduction, in fact, beyond improving metabolic stability by blocking metabolically labile sites, can modulate physicochemical properties, such as lipophilicity or acidity, change molecular conformation, and increase binding affinity by exploiting specific interactions of fluorine with the target protein.[29,30] However, as can be seen in Table 1, the introduction of fluorine

did not markedly affect the activity towards both PPARα and PPARγ in comparison with LT175 allowing to hypothesize the accommodation of this atom in a region which provides a small contribution to the complex with the receptor and therefore is not determinant for agonist activity.

The introduction of a double bond between the carbon alpha to the carboxylic group and the benzylic side chain led to the benzylidene analog **9**. The so obtained *Z* geometric isomer imposed a conformational constraint to the molecule, which, however, did not result particularly beneficial for activity. Probably, the lower flexibility and a higher degree of planarity compared to LT175 were not favorable for receptor activation causing a reduction of potency and efficacy on both PPARα and PPARγ subtypes. The next modification consisted in the increase of the size of benzyl aromatic nucleus of LT175 to naphthalene. This chemical modification was carried out to investigate the effects resulting from the introduction of a larger lipophilic aromatic moiety into the structure of LT175. The presence of a naphthalene could confer to a PPAR ligand peculiar pharmacological properties deriving from a different accommodation into the receptor pocket. In fact, as previously reported in the literature, some ligands containing this group are able to provide a unique interaction mechanism for stabilization of the complexes with both PPARα and PPARγ.[31,32] With this aim, we prepared compound **10**, which showed a very interesting dual pharmacological profile by acting as an equipotent PPARα full agonist and PPARγ partial agonist. Its efficacy towards both subtypes was very similar to that of LT175 even though with a slightly lower potency; but, once again, the resolution of the racemate should allow to discriminate between the enantiomers activities providing an eutomer endowed with higher potency and efficacy.

Finally, we decided to substitute the carboxylic function of LT175 by bioisosteric acylsulphonamide, sulphonamide or amide groups. This choice derived from the previously reported presence of these groups in a number of PPAR ligands, which often exhibit a particularly favorable activity profile towards PPARγ being able to uncouple the adverse effects from therapeutic effects.[33-39] For this purpose, we started from LT175 and prepared compounds **11-15**,

which, of course, were obtained as *S* isomers. The two acylsulphonamides **11** and **12** showed opposite effects; in fact, the methyl acylsulphonamide **11** acted basically as a PPARα partial agonist with very low activity towards PPARγ, whereas the corresponding *p*-tolyl derivative **12** behaved as an antagonist towards both PPARα and PPARγ subtypes. The antagonist activity of **12** was confirmed by conducting a competitive binding assay in which PPARα and PPARγ activity at a fixed concentration of the reference agonists Wy-14,643 and rosiglitazone, respectively, were measured in cells treated with increasing concentrations of **12**. These results allow to suppose that the presence of a *p*-tolyl group in place of a methyl hampers interactions with the residues that are critical for receptor activation due to steric hindrance. This effect was previously explained for some structurally similar PPAR ligands by a shift of helix H12 out of the agonist bound position inducing a PPAR-LBD conformation that interacts efficiently with corepressors.[40] As regards sulphonamides **13** and **14**, the former behaved as an antagonist towards both PPARα and PPARγ, whereas the latter showed antagonist activity only towards PPARα being completely inactive on PPARγ. These compounds lack the carbonyl group compared to acylsulphonamides **11** and **12** and this modification converted also the activity of the methyl derivative **13** from agonist to antagonist. Finally, the introduction of the anilido group in place of the carboxylic function of LT175 led to **15**; however, this derivative turned out to be completely devoid of any activity probably due to the lack of an acidic function, which results apparently important in this class of compounds.

Docking Studies. To investigate the molecular basis of the activity of compound **10**, which showed the best dual pharmacological profile, docking calculations were performed in the crystal structures of PPARα in complex with AL29-26 (PDB 5HYK)[32] and PPARγ in complex with LT175 (PDB 3B3K).[18] These structures were chosen because both co-crystallized ligands feature a bulky aromatic scaffold and a carboxylic acid moiety, similar to this series of derivatives. For compound **10**, both enantiomers, namely (*R*)-**10** and (*S*)-**10**, were considered. The results of the docking

protocol indicated a common binding mode for (*R*)- and (*S*)-**10** in PPARα. The two enantiomers were both positioned within arm I (a polar region extending toward H12), establishing a very tight network of H-bonds with the side chains of Y314, H440, S280 and Y464 on H12 (Figure 2A-B) through the carboxylic acid head group. Superposition of the docked poses of (*R*)- and (*S*)-**10** showed a very nice fit of their diphenyl moiety with the aromatic tail of the co-crystallized AL29-26 (Figure 2C). In particular, the aromatic diphenyl moiety filled the hydrophobic region between H3, H11 and H12, whose access is usually impaired by the presence of the aromatic ring of F273. This latter acts as a gatekeeper for the accommodation of rigid and bulky substituents.[32]

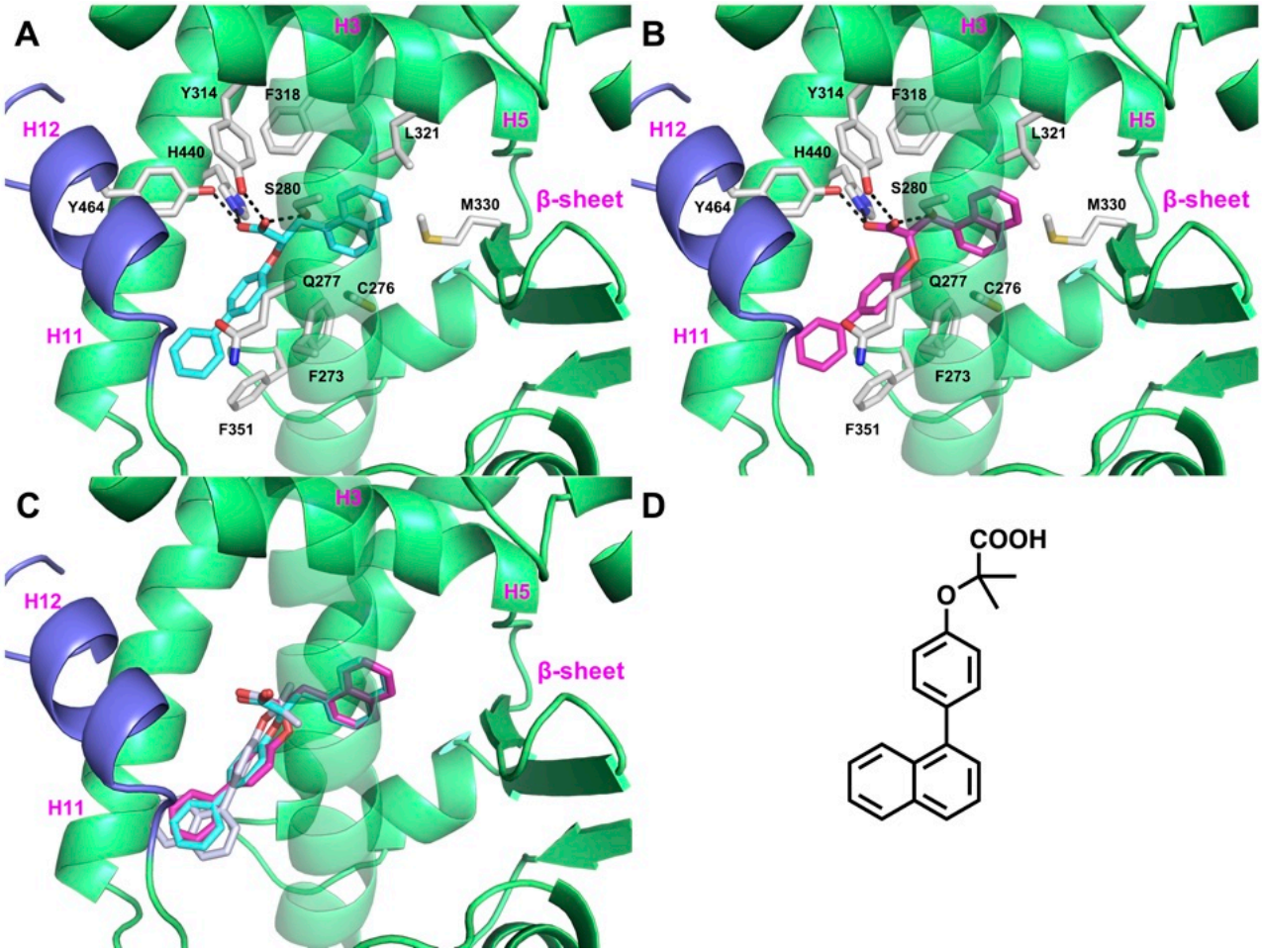

Figure 2. Binding mode of compounds (*S*)-**10** (A, cyan sticks) and (*R*)-**10** (B, magenta sticks) into PPARα LBD (green ribbons, PDB 5HYK). H12 is colored in slate. Only amino acids residues discussed in the main text are displayed (white sticks) and labeled. H-bonds discussed in the text are depicted as dashed black lines. (C) Overlay of (*S*)-**10** and (*R*)-**10** docked poses on AL29-26 (blue white sticks, PDB 5HYK) co-crystallized into PPARα LBD. (D) Structure of compound AL29-26.

This hydrophobic cavity in PPARα is homologous to the "diphenyl pocket" found in the LT175/PPARγ complex (PDB 3B3K).[18] In this complex, the conformational switch of the F282 side chain induced by the ligand was also observed.

The docking results revealed that (*S*)-**10** formed the well-recognized H-bonds with the side chains of Y473 on H12, H449, H323 and S289 in PPARγ arm I through its carboxylate group (Figure 3A). The docked pose of (*S*)-**10** superimposed well on the co-crystallized pose of LT175 (Figure 3C), with both diphenyl groups occupying the region normally hosting F282 in the apo-form of the receptor, and thus contributing to stabilize the loop 11/12. Differences in the hydrophobic packing of this loop may contribute to different H12 dynamics, inducing a conformation of the LBD less prone to the recruitment of coactivators required for full activation of PPARγ,[18] also influencing the expression of PPARγ target genes.[19]

On the other hand, (*R*)-**10** was found to bind within arm I as well, however the carboxylate group was positioned at a slightly higher distance from H12 and Y473 side chain, ($d_{OH\text{-}O2}$ = 3.6 Å; $d_{OH\text{-}O3}$ = 3.9 Å), establishing only two H bonds with S289 and Y327 side chains. Moreover, the ligand phenolic oxygen was at H-bonding distance from the C285 SH group. Thus, (*R*)-**10** engaged fewer interactions than (*S*)-**10** and rather stabilized H3 and H5. On the basis of these data, it is reasonable to hypothesize that (*S*)-**10** might represent the eutomer endowed with higher potency and efficacy, as also observed for LT175. It is worth noting that the *R* enantiomer of LT175 was previously

reported to bind in a different site with respect to LT175, in the region between H3 and the β-sheet of PPARγ,[18] as observed for other known partial agonists.[41]

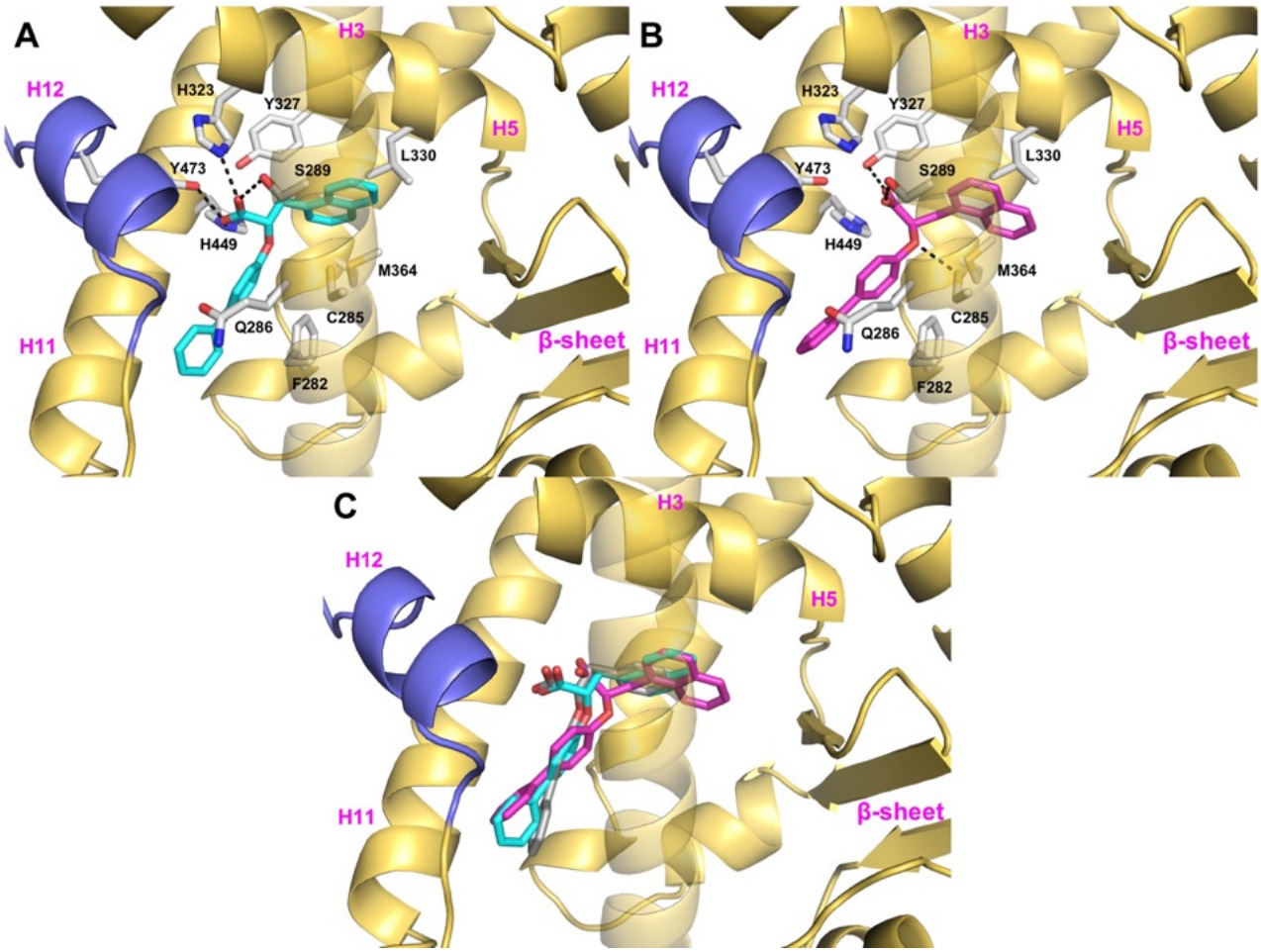

Figure 3. Binding mode of compounds (*S*)-**10** (A, cyan sticks) and (*R*)-**10** (B, magenta sticks) into PPARγ LBD (yellow ribbons, PDB 3B3K). H12 is colored in slate. Only amino acids residues discussed in the main text are displayed (white sticks) and labeled. H-bonds discussed in the text are depicted as dashed black lines. (C) Overlay of (*S*)-**10** and (*R*)-**10** docked poses on LT175 (gray sticks, PDB 3B3K) co-crystallized into PPARγ LBD.

However, the binding mode can be influenced by several experimental conditions, such as soaking time or concentration. In fact, crystal structures of PPARγ in complex with aryloxy phenyl propanoic acid derivatives showed that these ligands are able to sample both sites of the LBD[42] or

even to simultaneously occupy both sites of the receptor,[21] regardless of the configuration of the stereogenic center close to the carboxylic function. Thus, there might be the existence of an equilibrium between the two binding modes, as suggested by a recent study.[43]

The binding mode of **10** allowed us to derive possible insights about the SAR of this series of derivatives. The straight and rigid phenyl group in compound **1** (replacing the benzyl of LT175) would likely clash with residues on H5 (F318 in PPARα and Y327 in PPARγ), thus resulting in reduced potency toward both subtypes. The benzyl group elongation with two or three methylene units (derivatives **2** and **3**, respectively) improved activity in comparison with **1**, however only the benzyl group conferred the optimal distance for the establishment of fruitful hydrophobic interactions with a leucine residue acting as a "clamp", namely L321 in PPARα and L330 in PPARγ.

Elongation of the diphenyl moiety (compounds **4** and **5**) reduced both potency and efficacy, likely because the diphenyl pocket is rather tight. The modification of the stereogenic carbon by introducing a methyl group increased potency and efficacy on both subtypes, with derivative **6** showing an EC_{50} on PPARα similar to LT175 and a slightly higher EC_{50} on PPARγ. The methyl group was better tolerated in PPARα than in PPARγ, likely because this latter features a tighter turn of H3 imparted by a glycine residue (G284). The introduction of fluorine atoms on the benzyl group (derivatives **7** and **8**) caused a slight reduction of the potency while maintaining an efficacy similar to LT175. These data suggest that a bulkier and aromatic system like naphthalene in (*S*)-**10** is preferred over the substituted benzyl group, because of its ability to engage more extensive hydrophobic interactions within the LBD with, for instance, L321 in PPARα and L330 in PPARγ. The more constrained benzylidene of derivative **9** might well have an impact on the ligand's ability to transition from the entry site to arm I and transactivate the receptor, resulting in reduced activity.

Finally, modifications of the carboxylic head group led to weak/inactive PPAR agonists (compounds **11** and **15**) or even antagonists (compounds **12-14**). We have previously shown that

the introduction of sulfonimide and amide moieties in this position leads to an "agonist to antagonist switch",[40] as such head groups are able to push the H12 to assume an inactive and less structured conformation favoring the interactions with corepressors.

***In Vivo* Pharmacokinetic Study of Compound 10.** A bioavailability study of **10** was carried out in male Sprague-Dawley rats and the pharmacokinetic parameters are presented in Table 2. Following a single intravenous (IV) administration of **10** formulation at 1 mg/kg, the mean plasma clearance (Cl) was found to be low, 2.11 mL/min/kg, which is approximately 0.04-folds lower than normal hepatic blood flow of rats. The volume of distribution was found to be 2.27 L/kg, which was approximately 3.24-folds greater than total body fluids in rats (0.7 L/kg) indicating high distribution in tissues. The terminal plasma elimination half-life ($T_{1/2}$) was also found to be high (12.5 h).
After a single oral (PO) gavage administration of **10** formulation at 5 mg/kg, the median time to reach the maximum plasma concentration (T_{max}) was found to be 2 h. The exposure was found to be 1870 ng/mL (C_{max}) and 22700 h·ng/mL (AUC_{last}). The absolute oral bioavailability was 71.9%.

Table 2. Mean pharmacokinetic parameters following a single intravenous (IV) bolus and oral (PO) administration of **10** in male Sprague-Dawley rats.

Parameters	**Compound 10**	
	IV (1 mg/kg)	PO (5 mg/kg)
Dose Volume (mL/kg)	10	10
C_0/ C_{max} (ng/mL)	1650±352 (C_0)	1870±150 (C_{max})
T_{max} (h)	0.083	2
AUC_{last} (h·ng/mL)	6310±625	22700±683

$AUC_{infinity}$ (h·ng/mL)	7980±997	28900±3270
$T_{1/2}$ (h)	12.5±0.566	10.8±2.49
V_d (L/kg)	2.27±0.184	2.68±0.312
Cl (mL/min/kg)	2.11±0.262	2.91±0.319
MRT_{last} (h)	8.67±1.06	8.8±0.237
%F	--	71.9±2.22

C_0/C_{max}: maximum plasma concentration; T_{max}: time to reach the maximum plasma concentration; AUC_{last}: area under the curve from time zero to the last measurable concentration; $AUC_{infinity}$: area under the curve from time zero to infinity; $T_{1/2}$: plasma elimination half-life; V_d: volume of distribution; MRT_{last}: Mean Residence Time to the last concentration; Cl: plasma clearance; F: oral bioavailability.

In Vivo **Antihyperglycemic Screening.** Streptozotocin (STZ)-induced diabetic mice model was used to evaluate the antihyperglycemic activity of test compound **10** alone or in combination with reference standard pioglitazone. The test dose was fixed based on the predicted LD_{50} value.[44] Doses lower than $1/50^{th}$ and $1/100^{th}$ of predicted LD_{50} value were used for the study. Diabetic mice were orally treated with the test compound at a dose of 25 mg/kg (Group 3) and 50 mg/kg body weight (Group 4) for a period of 15 days. Fasting blood glucose level of control (Group 6), diabetic-untreated (Group 1) and diabetic-treated (Groups 2-5) mice was tested on day 0, 5, 10 and 15 of the screening period (Table 3). Data were statistically analyzed by one-way ANOVA followed by Dunnett's t-test using R-Package.

Compared to normoglycemic control (Group 6), diabetic control animals (Group 1) showed severe hyperglycemia. On day 0, the mean blood glucose level in the diabetic control group was 365±54.25 mg/dL and increased to a level of 435.2±46.89 - 456.8±63.77 mg/dL during the period from day 5 to 15. Treatment with the standard drug pioglitazone (30 mg/kg, Group 2) showed a gradual decrease in blood glucose level from day 5 to 15, which became significant at day 10 and 15 (248±25.97 and 224.2±28.28 mg/dL, respectively) compared to Group 1. Both treatments with

the test compound (Groups 3 and 4) gave similar results decreasing the blood serum glucose level in the diabetic mice particularly on 10^{th} and 15^{th} days with the lowest dose (Group 3) showing equivalent effects to 30 mg/kg pioglitazone. Given that no dose-dependent response was observed for **10**, we decided to evaluate a co-treatment (Group 5) with **10** (25 mg/kg) and pioglitazone (30 mg/kg). However, no additive effect was obtained, in fact, Group 5 showed basically the same significant decrease in blood glucose level of Groups 2 and 3.

Table 3. Effect of **10** on fasting blood glucose levels (mg/dL) in STZ-induced diabetic mice.

	Blood glucose level (mg/dL)			
Groups	Day 0	Day 5	Day 10	Day 15
1. Diabetic Control	365±54.25	456.8±63.77	435.2±46.89	452.6±48.94
2. Pioglitazone	441.2±35.62	351±51.88	248±25.97***	224.2±28.28***
3. **10** (25 mg/kg)	408±35.6	333.6±24.0	166.2±23.92***	135.6±23.78***
4. **10** (50 mg/kg)	280.6±11.4	162.2±22.34***	125.2±16.35***	111.2±5.89***
5. **10** + Pioglitazone	356.4±60.06	205±21.53**	118.2±11.58***	122.6±14.33***
6. Normal Control	87.6±8.79	86.6±8.48	86.4±9.29	86.6±7.77

***$p < 0.001$ *vs* diabetic control; **$p < 0.01$ *vs* diabetic control.

***In Vivo* Lipid Profiling.** Total cholesterol (TC), triglyceride (TG), high-density lipoprotein cholesterol (HDL-C), low-density lipoprotein cholesterol (LDL-C), and very low-density lipoprotein cholesterol (VLDL-C) levels were measured by collecting the blood before sacrificing the animals. STZ-induced diabetic mice (Group 1) displayed very high levels of TC, HDL, LDL, VLDL, and TG compared to the normal control group (Group 6). Oral treatment with **10** (25 mg/kg, Group 3) significantly reduced the levels of TC, HDL, LDL-C, VLDL-C, and TG bringing diabetes-induced hyperlipidemia back to normal. It also showed better anti-hyperlipidemic activity than the standard drug pioglitazone (Group 2). Unexpectedly, oral treatment with a higher dose of **10** (50 mg/kg, Group 4) revealed a similar reduction of HDL level compared to Group 3, but less reduction of TC, LDL, VLDL, and TG level. Co-treatment of Group 5 with **10** (25 mg/kg) and pioglitazone (30 mg/kg) produced only a better reduction of VLDL and TG level compared to all other treated groups (Table 4).

Table 4. Effect of **10** on lipid profile in STZ-induced diabetic mice.

	Blood lipid level (mg/dL)				
Groups	TC	HDL	LDL	VLDL	TG
1. Diabetic Control	184.3±1.2	43.3±1.2	113.3±0.4	27.8±0.2	139.3±0.9
2. Pioglitazone	88.7±2.6	19.7±0.9***	20.5±0.1***	19.3±0.3***	98.3±0.3***
3. **10** (25 mg/kg)	66.3±0.9***	23.0±2.1***	25.6±0.4***	15.4±0.1***	76.3±1.2***
4. **10** (50 mg/kg)	86.0±1.2*	22.7±2.3***	42.2±0.3***	21.1±0.1***	104.0±0.9***
5. **10** + Pioglitazone	76.3±1.4**	15.7±0.9***	48.3±0.1***	11.5±0.2***	57.3±1.2***
6. Normal Control	59.0±0.6	22.3±0.3	21.3±0.2	15.6±0.2	78.7±0.9

***$p < 0.001$ *vs* diabetic control; **$p < 0.01$ *vs* diabetic control; *$p < 0.05$ *vs* diabetic control.

Histopathological Studies of Bone, Kidney and Liver. These studies were conducted in order to evaluate possible toxic effects of **10** on these tissues. In fact, it is known that the use of PPARα/γ agonists, especially if they produce a full activation, is often associated with unwanted effects such as bone fractures, renal disease, and liver dysfunction.[45-47]

Histopathological observations of bone, kidney and liver were carried out at 40x magnifications using hematoxylin and eosin (HE) staining. The effects of **10** and pioglitazone on bone, kidney and liver tissues are shown in Figures 4, 5, and 6, respectively.

Microscopic examinations of the normal bone tissue of the non-diabetic mice revealed normal architecture of bone with normal density. By contrast, STZ-induced diabetic mice showed low bone density, which clearly indicated resorption in bone tissue (Figure 4). However, a section of bone tissue in the treated Groups 2-5 of mice showed improvement in bone density compared to diabetes control group (Figure 4). Histopathological assessment of the normal kidney of the non-diabetic mice showed normal renal cortex, glomerular tufts, proximal tubules and distal tubules. As expected, kidney section of STZ-induced diabetic mice showed shrinked glomeruli and distorted proximal and distal tubules (Figure 5). However, a kidney section of treated Groups 2 and 3 showed healthy morphology of these cellular components as a clear consequence of drug effect, whereas Groups 4 and 5 presented only a slight distortion of proximal and/or distal tubules (Figure 5).

Histopathological assessment of the normal liver tissue of the non-diabetic mice confirmed the normal structure of the liver. Each lobule consisted of interconnecting plates of epithelial cells called hepatocytes, which were radially arranged around a central vein (Figure 6). In contrast, liver sections of STZ-induced diabetic mice disclosed hepatocellular damage consisting in liver architectural distortion, fibrosis, inflammation and leucocyte infiltration around the central vein (Figure 6). Sections of the liver in diabetic rats treated with **10** or pioglitazone, either alone or in combination, showed an improved morphology similar to that of the healthy group (Figure 6).

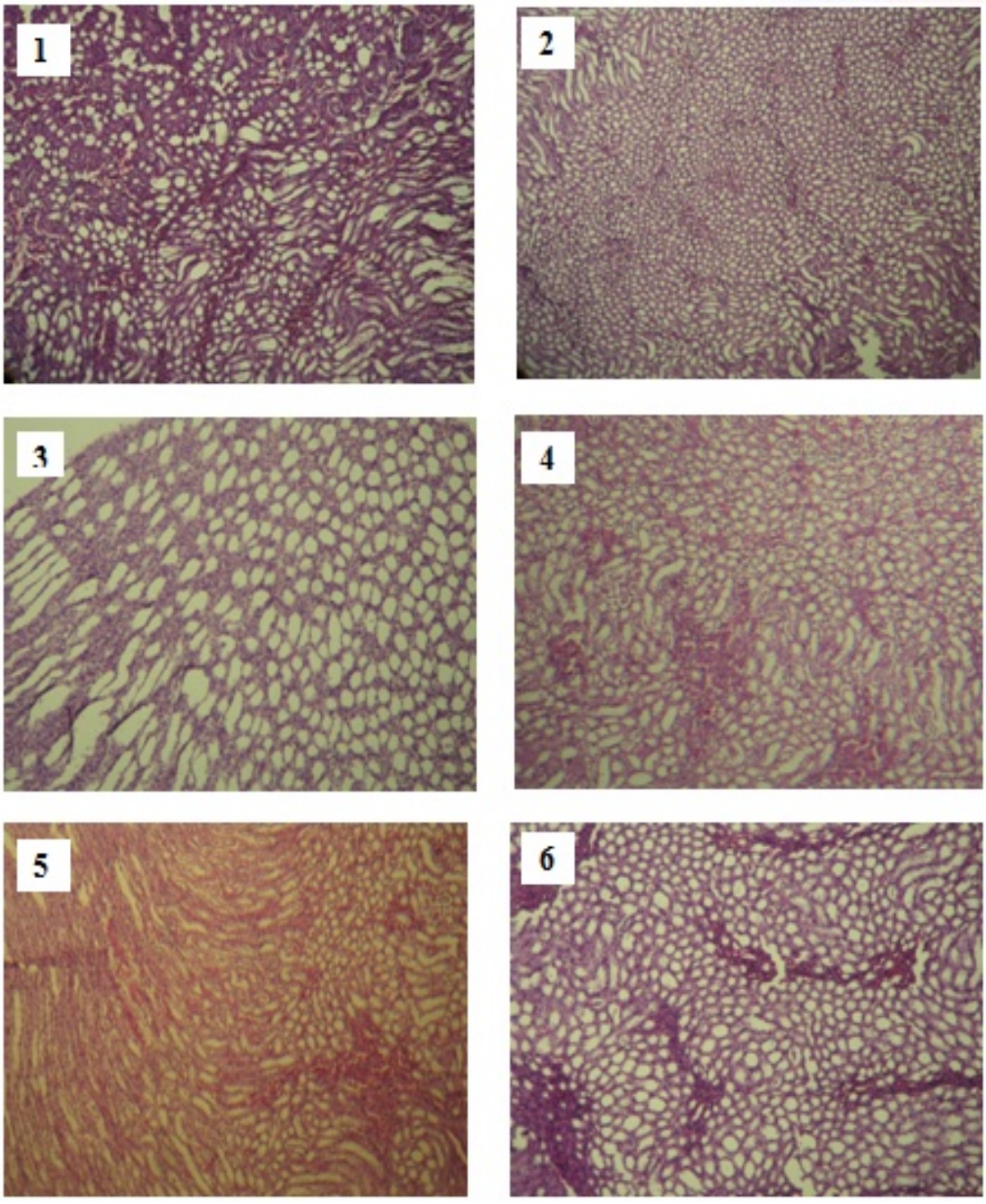

Figure 4. Histopathology of the bone. Light micrographs of bone sections from the different Groups. The numbers on the images represent the Groups according to the text**.** Diabetic untreated Group (1) revealed marked decrease in bone density. Bone density of treated Groups (2-5) looks healthy in comparison with normal Group (6). Examinations were carried out at 40x magnifications with hematoxylin-eosin's staining.

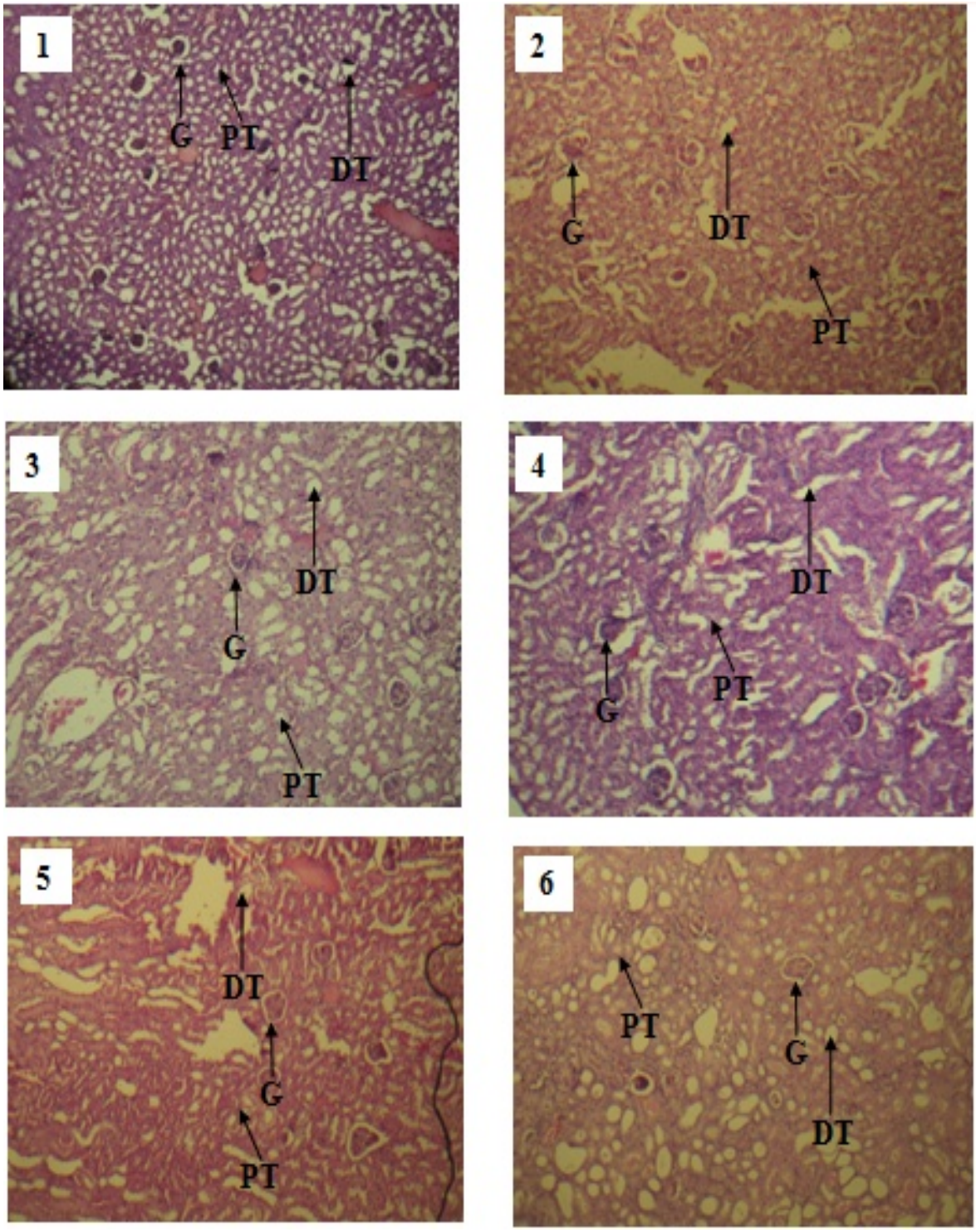

Figure 5. Histopathology of the kidney. Light micrographs of kidney sections from the different Groups. The numbers on the images represent the Groups according to the text. Diabetic untreated Group (1) showed shrinked glomeruli (G) and distorted proximal (PT) and distal tubules (DT). Groups 2 and 3 revealed healthy conditions of G, PT and DT; Group 4 showed normal glomeruli, but distorted DT and PT, whereas Group 5 presented normal conditions of G and PT, but slightly distorted DT compared to normal Group (6). Examinations were carried out at 40x magnifications with hematoxylin-eosin's staining.

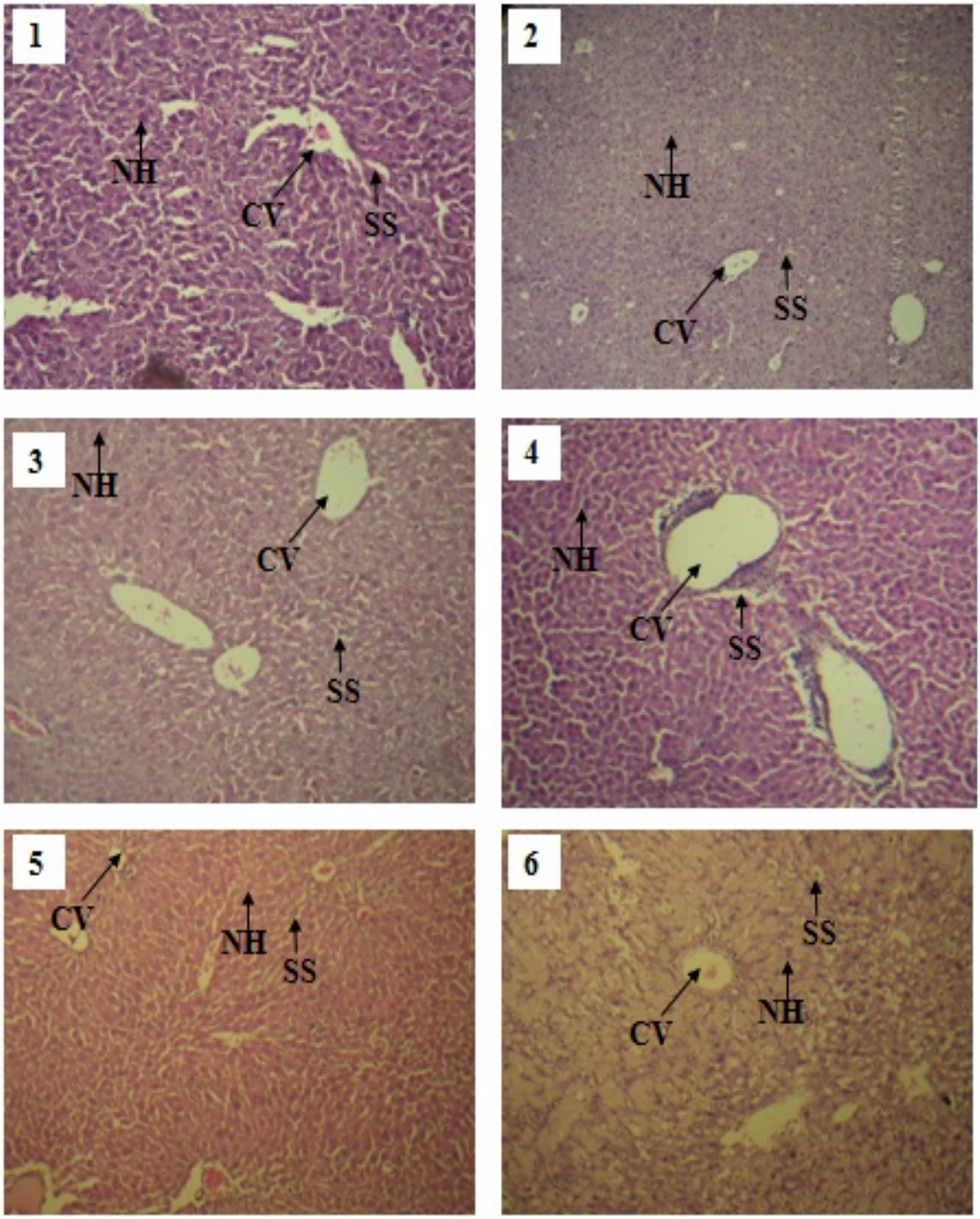

Figure 6. Histopathology of the liver. Light micrographs of liver sections from treated and untreated Groups. The numbers on the images represent the Groups according to the text. Diabetic control mouse liver section (1) showing severe damaged hepatic architecture with damaged central vein (CV), elevated sinusoidal space (SS) and distorted normal hepatocytes (NH). In Group 2 pathological condition is almost back to normal. Group 3 showed normal condition of CV, NH as well as SS. Group 4 showed healthy CV and NH surrounding CV, but slightly increased sinusoidal space. Group 5 looked healthy with normal condition of CV, NH and SS similar to the normal control Group 6. Examinations were carried out at 40x magnifications with hematoxylin-eosin's staining.

Effects of Compound 10 on Glucose Uptake. The effects of compound **10** on glucose and lipid levels can be certainly ascribed, at least in part, to PPARα/γ activity. However, the structural similarity of this compound with ertiprotafib, a well-known molecule showing a concomitant activity as protein tyrosine phosphatase 1B (PTP1B) inhibitor,[29] prompted us to evaluate the possible effects of **10** on this target. PTP1B is a negative regulator of insulin and leptin signaling pathways[48,49] and it is universally recognized as one of the most promising pharmacological targets for the treatment of type 2 diabetes.[50] Administration of PTP1B inhibitors to diabetic mice models improved the sensitivity to insulin and showed normalization of glycaemia and loss of body weight in obese mice.[49] Therefore, we carried out in vitro kinetic assays, which demonstrated that **10** effectively inhibited PTP1B, showing an IC_{50} of 13.2 ± 1.2 μM (Figure S1 of S.I.). However, when we analyzed the effect of **10** on insulin signaling pathway by using C2C12 muscle cells, we found that the treatment did not produce a significant increase of phosphorylation status of Akt, a downstream substrate of insulin receptor activation, neither alone nor in combination with insulin (Figure S2 of S.I.). Surprisingly, these data were in contrast with in vitro kinetic assays showing that **10** acted as a good PTP1B inhibitor. At this point, we decided to evaluate whether **10** acted by enhancing the activity of glucose transporter GLUT4 or activating AMPK, an enzyme that plays a crucial role in cellular energy homeostasis by promoting glucose and fatty acid uptake and oxidation. Therefore, we conducted further tests by measuring glucose uptake in C2C12 cells pre-treated with 10 μmol Cytochalasin B or Compound C, which are potent inhibitors of GLUT4 and AMPK, respectively. However, data reported in Figure S3 of S.I. showed that **10**-induced glucose uptake was not influenced by treatment with Cytochalasin B or Compound C, confirming that it did not act by enhancing GLUT4 transport rate or AMPK activity. These data allowed to hypothesize that the increased absorption of glucose could occur through mechanisms which did not involve insulin. To confirm this hypothesis, we evaluated if the acute treatment with **10** was able to stimulate the upload of 2-NBDG in C2C12 cells. Cytofluorimetry analysis of C2C12 cells treated with insulin, **10** or insulin-**10** combination showed that **10** strongly enhanced the uptake of glucose

in an insulin-independent mechanism, as demonstrated by evidence that **10**-insulin co-stimulation did not increase glucose uptake compared to treatment with **10** alone (Figure 7). At the same time, in this experiment we proved that **10** strongly increased glucose uptake after only 30 minutes. This acute effect suggested that the enhanced glucose transport activity might not be entirely explained by transcriptional events associated with PPAR activation.

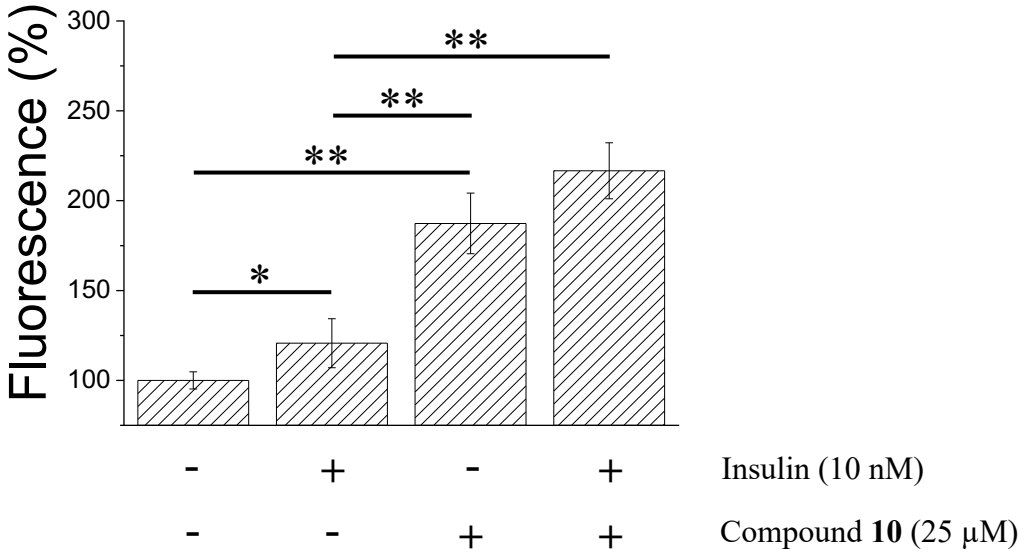

Figure 7. Glucose uptake assay. C2C12 myoblasts were starved for 24 h and then incubated for 30 min with starvation medium containing 25 μM **10**, 10 nM insulin or the combination **10**-insulin. After this time, cells were washed with PBS and incubated with starvation medium containing 40 μM 2-NBDG for 3 h. Finally, cells were washed, tripsinized and analyzed using a flow cytometry. All test was carried out in triplicate. Data obtained were normalized respect to control sample and reported as the mean ± SD. The differences between series of data were statistically analyzed using the Unpaired Student's T test. p values ≤ 0.05 were considered statistically significant (* $p < 0.05$, ** $p < 0.01$).

As reported above, the TZD drugs act as insulin sensitizers and are agonists of PPARγ, which mediates many of their beneficial effects. However, TZDs are known to interact with additional molecular targets and can affect metabolism by mechanisms other than transcription regulation.

Indeed, recent papers have suggested that beyond classical TZDs like rosiglitazone and pioglitazone, also TZDs with very limited activation of PPARγ (PPARγ-sparing TZDs) have beneficial metabolic effects. This PPARγ-independent pharmacology has been linked to the ability of these compounds to interact with the mitochondrial pyruvate carrier (MPC) complex.[51-54] MPC is a heterodimeric complex that mediates the transport of pyruvate across the inner mitochondrial membrane into the mitochondrial matrix. This is an important and rate-limiting step in intermediary metabolism and its inhibition results in protection from diabetes, liver injury, and other high-fat (HF) diet–induced metabolic derangements.[55] For this purpose, we decided to compare the effects on glucose uptake of our compound **10** with UK5099 (Figure 8), a mitochondrial pyruvate transporter inhibitor. Data showed in Figure 8 confirmed that in C2C12 cells the treatment with UK5099 generated results similar to that obtained after treatment with **10**, improving the glucose uptake with an insulin-independent mechanism. Interestingly, **10** turned out to be much more efficient than UK5099 given that the dose needed to stimulate the absorption of an equivalent amount of 2-NBDG was 800 times lower than that of UK5099.

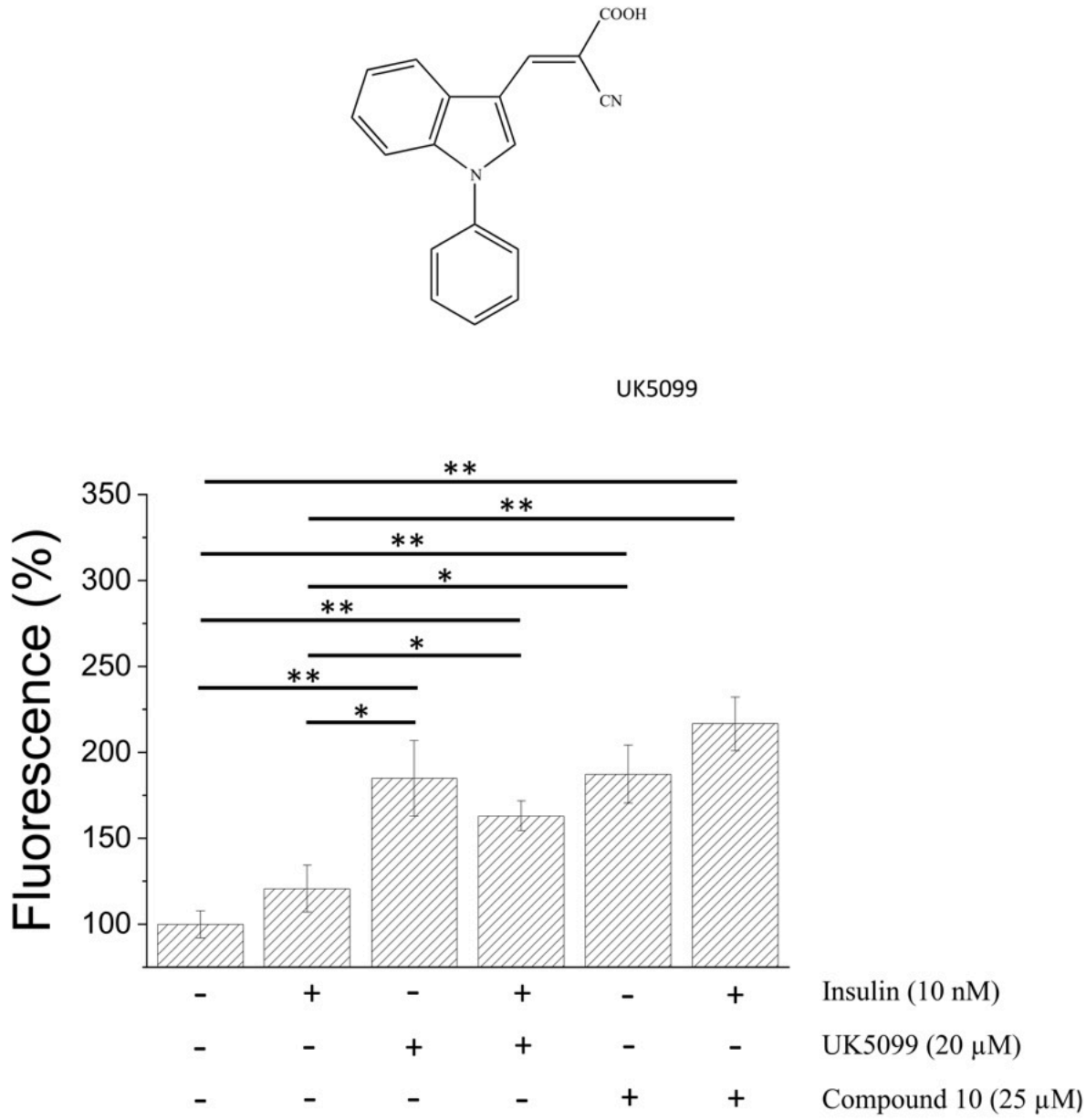

Figure 8. Glucose uptake assay. C2C12 cells were starved for 24 h and then incubated for 30 min in the presence of 10 nM insulin, 25 µM **10**, 20 µM UK5099 or with the UK5099-insulin and **10**-insulin combinations. After this time, cells were washed with PBS and incubated with fresh starvation medium containing 40 µM 2-NBDG for 3 h. Finally, cells were detached and analyzed using a flow cytometer. Each test was carried out in triplicate; 10.000 events were analyzed for each experiment. Data showed in the figure represent the mean value ± SD (n=3). Unpaired t test was carried out to evaluate the significance between samples. * $p < 0.05$; ** $p < 0.01$.

At this point, to evaluate the possible inhibition of MPC by **10**, we studied the bioenergetics profile of C2C12 cells by using the Seahorse technology. In fact, it has been reported that treatment with UK5099 decreased oxygen consumption and ATP/AMP ratio value of C2C12, thereby inducing the activation of AMPK.[54] However, treatment with **10** did not decrease either basal oxygen consumption or ATP production-related oxygen consumption and did not affect spare capacity and maximal mitochondrial respiration. Interestingly, we observed only a slight, but significant increase in proton leak following the treatment with **10**, which, in contrast, remained unchanged after treatment with UK5099 (Figure 9). Considering that an increase in proton leak is frequently related to a loss of mitochondrial membrane potential, we investigated this aspect by analyzing the mitochondrial membrane potential of C2C12 cells treated with **10**, UK5099, and FCCP (carbonyl cyanide 4-(trifluoromethoxy)phenylhydrazone) a potent mitochondrial oxidative phosphorylation uncoupler, which was used as a positive control (Figure 10). As expected, FCCP treatment caused a decrease of the mitochondrial membrane potential. Moreover, we found that the treatment with **10** produced effects similar to FCCP, whereas the treatment with UK5099 resulted in a lower reduction in mitochondrial membrane potential. Interestingly, pre-treatment of C2C12 cells with methyl pyruvate, which is a freely diffusible form of pyruvate, caused a complete rescue of membrane potential in C2C12 cells treated with UK5099 and **10**, but not in cells treated with FCCP (Figure 10). These results reinforce the hypothesis that **10** acts as an inhibitor of mitochondrial pyruvate carrier.

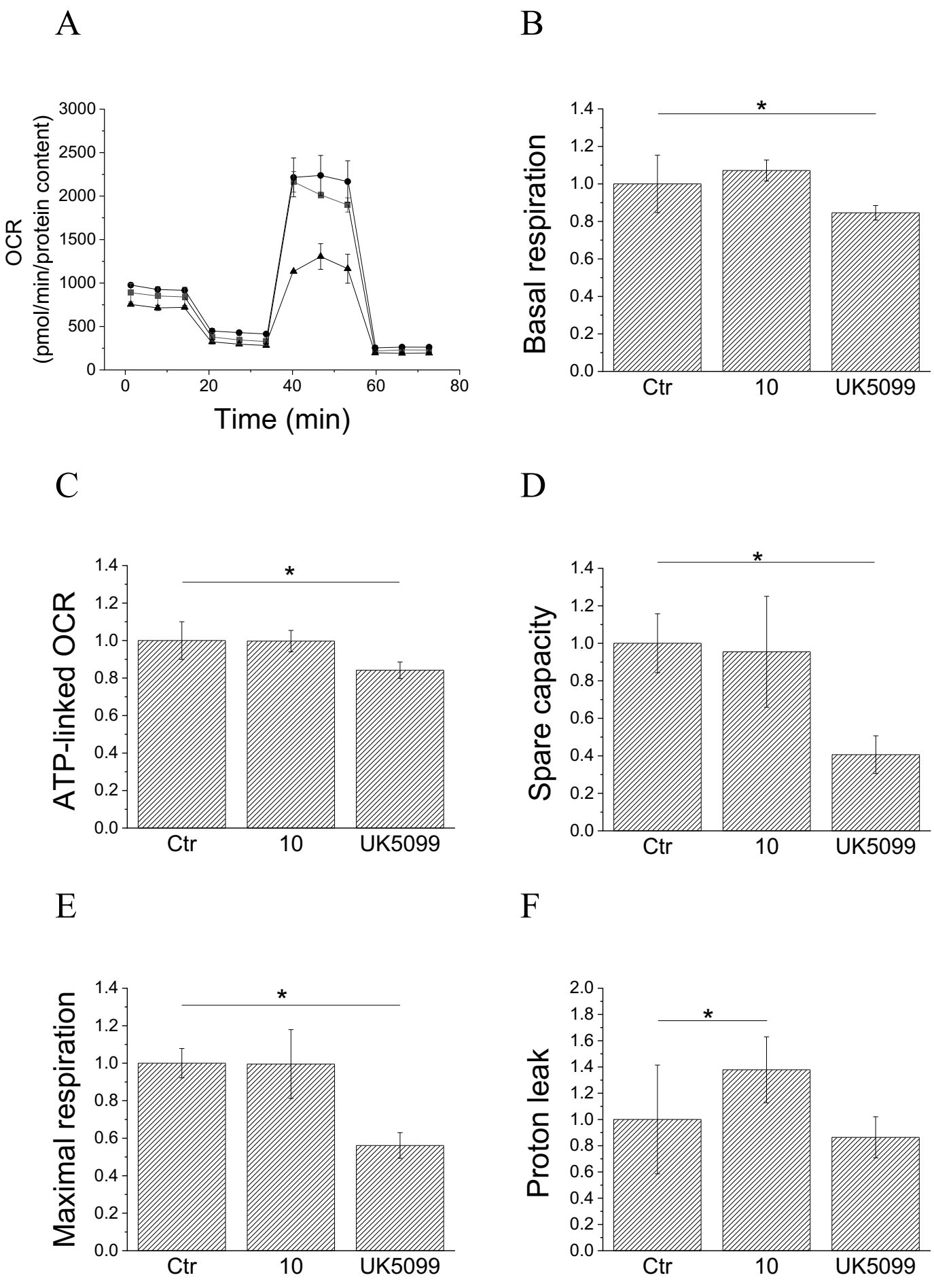
A
B
C
D
E
F
OCR
(pmol/min/protein content)
Time (min)
Basal respiration
ATP-linked OCR
Spare capacity
Maximal respiration
Proton leak
Ctr
10
UK5099
*

Figure 9. Seahorse XF Cell Mito Stress Test profile. $3x10^4$ C2C12 cells were plated in XFe96 cell culture plates. Mito stress analysis was carried out following the instructions of manufacturer to analyze the oxygen consumption rate (OCR). (A), Simbols used were: (■), untreated C2C12 cells; (●), C2C12 treated with 25 μM compound **10**; (▲), C2C12 cells treated with 20 μM UK5099. Data concerning basal respiration (B), ATP-linked OCR (C), spare capacity (D), maximal respiration (E), and proton leak (F) were determined using data reported in the figure (A). ATP-linked OCR was calculated after administration of the adenosine triphosphate ATP synthase inhibitor oligomycin, the spare capacity after administration of the proton uncoupler carbonyl cyanide 4-(trifluoromethoxy)phenylhydrazone (FCCP), and maximal respiration after administration of the combination of the respiratory complex I inhibitor rotenone and the respiratory complex III inhibitor antimycin A. Data showed in the figure represent the mean value ± SD (n = 3 or 4).
* indicates p value ≤ 0.05.

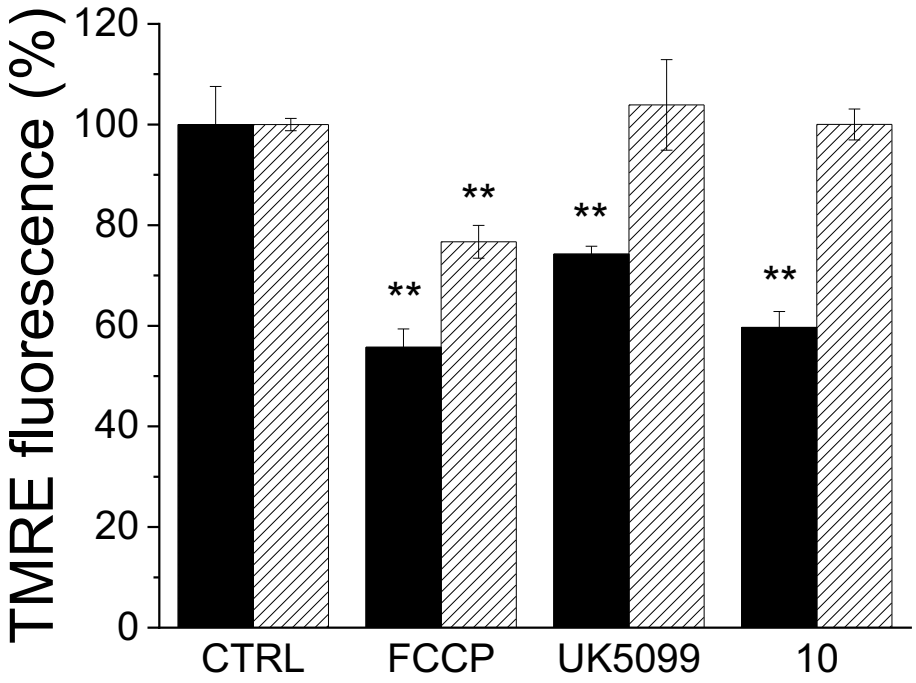

Figure 10. Evaluation of mitochondrial membrane potential using the TMRE probe. C2C12 cells were grown until 80% confluence and then starved for 24 h. After this time, cells were incubated with 2 μM FCCP for 10 min, or with 20 μM UK5099, or 25 μM **10** for 30 min, with/without 20 mM methyl pyruvate. Cells were washed with PBS and incubated in the presence of 100 nM of TMRE for 30 min. After this time, cells were detached and analyzed using a flow cytometer.

Unpaired t test was carried out to evaluate the significance between samples. * $p < 0.05$; ** $p < 0.01$.

Finally, we evaluated the acute cytotoxicity of **10** on myoblasts. For this purpose, C2C12 cells were incubated in the presence of 25 μM **10** for 7 h and then analyzed to evaluate their viability. Both MTT and crystal violet assays showed that this treatment did not significantly alter cell viability (Figure S4 of S.I.).

CONCLUSIONS

In conclusion, here we present evidence that compound **10** behaves as a well-tolerated antidiabetic agent, lowering blood glucose and lipids levels in diabetic mice models. Moreover, in the attempt to define the mechanism of action of **10**, we demonstrated that such compound behaves as a multitarget drug, acting as a PPARα/γ dual agonist and as inhibitor of mitochondrial pyruvate carrier (MCP). This finding is very interesting as recent studies have shown that other well-known antidiabetic compounds such as rosiglitazone specifically and acutely inhibit MPC. Therefore, we hypothesize that the glucose and lipid-lowering activity of **10** could also be triggered by the alteration of mitochondrial metabolism. In the past, different studies demonstrated that MCP inhibition is an affordable strategy to control energetic metabolism of cells. This inhibition impairs pyruvate availability, reduces oxygen consumption and mitochondrial ATP production.[56] Consequently, in an attempt to compensate for the drop in ATP, cells treated with MPC inhibitors increase the uptake and metabolism of glucose and amino acids such as glutamate and alanine. In these conditions, most of pyruvate generated by glycolysis is converted to lactate and then extruded in the extracellular milieu, while tricarboxylic acid cycle is sustained through the amino acid metabolism. Meanwhile, glutamate is rapidly converted into α-ketoglutarate and then converted in oxalacetate that can be used to metabolize the Acetyl-CoA generated by degradation of fatty acids.[57] Furthermore, MPC inhibition strongly impairs the ability of liver cells to convert pyruvate into glucose through gluconeogenesis, the metabolic pathway that often contributes to

hyperglycemia in diabetic patients.[58] Taken together, this evidence suggests that MPC inhibitors could be used as antidiabetic and antilipidemic agents.

Here we have shown that in murine myoblasts acute treatment with **10** induces, in the same way as UK5099, a rapid increase in glucose uptake, a phenomenon too rapid to be attributable to the ability of **10** to act as a PPAR agonist. Moreover, we have demonstrated that **10** in vitro inhibits PTP1B, one of the main negative regulators of insulin receptor. Although these results suggest that it can also act as an insulin sensitizing agent, the tests performed on C2C12 cells showed that it is unable to enhance the insulin signaling pathway, stimulate translocation of GLUT4 to the plasma membrane or activate AMPK, confirming that **10** does not work as an insulin sensitizing agent.

To evaluate the efficacy of **10** as an MPC inhibitor, we compared its activity with that of UK5099. It has been shown that in neurons grown in the presence of glucose and pyruvate, treatment with UK5099 resulted in an increase of glycolytic flux, but reduced oxygen consumption and oxygen-dependent ATP production, thus leading to the activation of AMPK. This finding suggests that increased glycolytic flux is unable to meet overall ATP demand in response to acute treatment with UK5099.[59] Similar results were obtained treating human skeletal muscle myotubes with UK5099.[54] Noteworthy, results of mito-stress assay that we carried out on C2C12 cells treated with UK5099 and reported in this manuscript substantially recapitulate results described in the Divakaruni study.[54] In fact, we observed that treatment with UK5099 reduced basal oxygen consumption, ATP-linked oxygen consumption rate, maximal respiration and spare capacity in C2C12 cells. Interestingly, none of these effects were observed after acute treatment with **10**; the only effect observed was a slight but significant increase in proton loss compared to both control cells and those treated with UK5099. Finally, we demonstrated that acute treatment with **10** and UK5099 reduced the mitochondrial membrane potential; interestingly, this effect was avoided by pretreatment of the muscle cells with methyl pyruvate, a permeable molecule which, once penetrated into the mitochondria, is converted into pyruvate thanks to the action of mitochondrial esterases. Taken together these results confirmed that **10** inhibits MPC, limiting pyruvate entry into

mitochondria. Whether loss of membrane mitochondrial potential is due to reduced pyruvate metabolism or to proton leak induced by **10**, remains to be elucidate.

The reason why the whole bioenergetics profile of C2C12 cells remained substantially unaffected after acute treatment with **10**, also remains an unresolved question. A possible explanation could lie in the hydrophobic nature of this compound, which could favor its localization into the membrane of muscle cells, hindering its diffusion into the cytoplasm and preventing its interaction with PTP1B. However, despite its low bioavailability, it can reach a cytoplasmic concentration sufficient to activate PPARs (EC_{50} around 1 μM) and to inhibit MPC in such a way to induce only a small reduction in mitochondrial potential. In the same moment, a small amount of **10** could interact with mitochondrial membrane, resulting in a small but significant increase of proton leak. Obviously, it cannot be ruled out the possibility that other mechanisms occur alternatively or in concomitance with MPC inhibition. As far as we know, this is the first PPARα/γ dual agonist reported to show this inhibitory effect. Next step will be the resolution of the racemic mixture that will allow to confirm the predicted better activity of the *S* enantiomer compared to the *R* one, as shown by our docking studies. This work is in progress as well as further studies to gain insight into the properties and biological action of this molecule, which may represent the potential lead of a new class of drugs with better and safer therapeutic effects in the treatment of dyslipidemic type 2 diabetes.

EXPERIMENTAL SECTION

Chemical Methods. Chemicals were used without any further purification and purchased from common suppliers. Column chromatography was performed using Fluka silica gel 60 Å as stationary phase. Melting points of solid compounds (uncorrected) were determined in open capillaries on a Gallenkamp electrothermal apparatus. Mass spectra were recorded on a HP MS6890-5973 MSD spectrometer equipped with a HP ChemStation or with an Agilent LC-MS 1100 Series. For exact mass analyses, in particular, we employed an LC-MSD Trap System VL spectrometer equipped with electrospray ionization (ESI). ^{1}H-NMR spectra were recorded using suitable deuterated solvents on a Varian Mercury 300 NMR Spectrometer or an Agilent VNMRS500. Chemical shifts (δ) are expressed as parts per million (ppm) and coupling constants (J) are expressed in Hertz (Hz). Optical rotations were measured with a PerkinElmer 341 polarimeter at room temperature (20 °C): concentrations are expressed as grams per 100 mL. The purity of all tested compounds was >95%, as confirmed by combustion analysis carried out with a Eurovector Euro EA 3000 model analyzer.

Synthesis of Diethyl 2-[(1,1'-biphenyl)-4-yloxy] malonate (**16**). To a solution in acetone (90 mL) of sodium 4-phenylphenate (23.4 mmol, 1.1 eq), prepared from an equivalent amount of 4-phenylphenol and sodium in absolute EtOH, diethyl 2-bromomalonate (21.37 mmol, 1 eq) dissolved in acetone (20 mL) was added dropwise. The reaction was stirred under reflux overnight. Then, the solvent was distilled off and the residue dissolved in ethyl acetate. The organic solution was washed with 2M NaOH and brine, dried over anhydrous Na_2SO_4, filtered and evaporated under reduced pressure to give a solid that was chromatographed twice on silica gel column (first *n*-hexane/ethyl acetate 80:20, and then CH_2Cl_2/*n*-hexane 80:20 as eluents) obtaining a white solid; yield 12%. ^{1}H-NMR (300 MHz, $CDCl_3$) δ (ppm): 1.32 (t, J = 7.0 Hz, 6H, $2CH_3$), 4.33 (q, J = 7.0 Hz, 4H, $2CH_2$),

5.24 (s, 1H, CH), 7.02 – 7.07 and 7.29 – 7.55 (m, 9H, aromatics); GC-MS *m/z* (%): 328 (100) $[M]^+$, 209 (24), 169 (44), 152 (44).

General Procedure for the Synthesis of 2a, 3a, 7a, 8a and 10a. NaH powder (1.6 mmol, 2 eq) was suspended in anhydrous DMF (5 mL), then **16** (0.80 mmol, 1 eq) dissolved in anhydrous DMF (5 mL) was added at 0 °C. After 30 min, the appropriate arylalkyl bromide (0.96 mmol, 1.2 eq), dissolved in anhydrous DMF (5 mL), was added dropwise. The reaction was stirred under inert atmosphere at 80 °C overnight. Then, DMF was distilled off and the residue dissolved in ethyl acetate. The organic solution was washed with aqueous solution of NH_4Cl and brine, dried over anhydrous Na_2SO_4, filtered and evaporated under reduced pressure. The resulting crude product was purified by chromatography on silica gel column.

*Diethyl 2-[(1,1'-biphenyl)-4-yloxy]-2-phenethylmalonate (**2a**).* Starting from (2-bromoethyl) benzene, eluent *n*-hexane/ethyl acetate 70:30 and CH_2Cl_2/*n*-hexane 60:40. The title compound was obtained as a colorless oil, yield 20%. ^{1}H-NMR (300 MHz, $CDCl_3$) δ (ppm): 1.25 (t, J = 7.0 Hz, 6H, $2CH_3$), 2.57 – 2.77 (m, 4H, $PhCH_2CH_2$), 4.27 (q, J = 7.0 Hz, 4H, $2COOCH_2$), 7.04 – 7.56 (m, 14H, aromatics); GC-MS *m/z* (%): 432 (36) $[M]^+$, 282 (33), 170 (80), 91 (100).

*Diethyl 2-[(1,1'-biphenyl)-4-yloxy]-2-(3-phenylpropyl)malonate (**3a**).* Starting from (3-bromopropyl) benzene, eluent *n*-hexane/ethyl acetate 80:20. The title compound was obtained in 67% yield. ^{1}H-NMR (500 MHz, $CDCl_3$) δ (ppm): 1.21 (t, J = 6.9 Hz, 6H, $2CH_3$), 1.72 – 1.79 (m, 2H, $CH_2CH_2CH_2$), 2.30 – 2.33 (m, 2H, CH_2Ph), 2.60 – 2.63 (m, 2H, CH_2CH), 4.24 (q, J = 6.9 Hz, 4H, $2COOCH_2$), 7.10 – 7.16, 7.21 – 7.32, 7.40 – 7.45 and 7.53 – 7.55 (m, 14H, aromatics); GC-MS *m/z* (%): 446 (42) $[M]^+$, 170 (100), 129 (29), 91 (29).

*Diethyl 2-[(1,1'-biphenyl)-4-yloxy]-2-(2-fluorobenzyl)malonate (**7a**).* Starting from 2-fluorobenzyl bromide, eluent *n*-hexane/ethyl acetate 90:10. The title compound was obtained as a yellow oil, yield 68%. ^{1}H-NMR (300 MHz, $CDCl_3$) δ (ppm): 1.16 (t, J = 7.0 Hz, 6H, $2CH_3$), 3.73 (s, 2H, $PhCH_2$), 4.20 (q, J = 7.0 Hz, 4H, $2COOCH_2$), 6.97 – 7.07, 7.19 – 7.39, 7.41 – 7.56 (m, 13H, aromatics); GC-MS *m/z* (%): 436 (65) $[M]^+$, 170 (100), 109 (34).

*Diethyl 2-[(1,1'-biphenyl)-4-yloxy]-2-(4-fluorobenzyl)malonate (**8a**).* Starting from 4-fluorobenzyl bromide, eluent *n*-hexane/ethyl acetate 90:10. The title compound was obtained as a yellow oil, yield 68%. ^{1}H-NMR (300 MHz, $CDCl_3$) δ (ppm): 1.15 (t, J = 7.0 Hz, 6H, $2CH_3$), 3.62 (s, 2H, $PhCH_2$), 4.19 (q, J = 7.0 Hz, 4H, $2COOCH_2$), 6.92 – 7.05, 7.18 – 7.39, 7.41 – 7.56 (m, 13H, aromatics); GC-MS *m/z* (%): 436 (43) $[M]^+$, 170 (100), 109 (56).

*Diethyl 2-[(1,1'-biphenyl)-4-yloxy]-2-(naphthalen-1-ylmethyl)malonate (**10a**).* Starting from 1-(bromomethyl) naphthalene, eluent *n*-hexane/ethyl acetate 90:10. The title compound was obtained in 40% yield. ^{1}H-NMR (300 MHz, $CDCl_3$) δ (ppm): 1.04 (t, J = 7.1 Hz, 6H, $2CH_3$), 4.02 – 4.17 (m, 6H, $2COOCH_2$ + $NaphCH_2$), 6.95 – 7.06, 7.27 – 7.59, 7.74 – 7.86 and 8.13 – 8.24 (m, 16H, aromatics); GC-MS *m/z* (%): 468 (31) $[M]^+$, 153 (99), 141 (100).

General Procedure for the Synthesis of 2, 3, 7, 8 and 10. 1M NaOH (2.5 mL, 5 eq) was added to a solution of **2a, 3a, 7a**, **8a** or **10a** (0.33 mmol, 1 eq) in absolute ethanol (5 mL). The resulting mixture was stirred under reflux overnight. The organic solvent was removed under reduced pressure, the aqueous residue was acidified with 2M HCl and then extracted with diethyl ether (three times). The collected organic portions were washed with brine, dried over anhydrous Na_2SO_4, filtered and concentrated to dryness. The resulting oil was heated at 160 °C and the crude product was crystallized from *n*-hexane/$CHCl_3$.

*2-[(1,1'-Biphenyl)-4-yloxy]-4-phenylbutanoic acid (**2**).* The title compound was obtained from **2a** as a white solid; yield 49%, mp 139 – 140 °C. ^{1}H-NMR (300 MHz, $CDCl_3$) δ (ppm): 2.32 – 2.37 (m, 2H, *CH_2*CH), 2.81 – 2.93 (m, 2H, PhCH_2), 5.7 (dd, 1H, J_1=7.0 Hz, J_2=5.7 Hz, CH), 6.95 – 7.02 and 7.18 – 7.55 (m, 14H, aromatics). HRMS ($C_{22}H_{20}O_3$-H)$^-$: calculated 331.1340, found 331.1337. Anal. Calcd for $C_{22}H_{20}O_3$: C, 79.50; H, 6.06. Found: C, 79.28; H, 6.37.

*2-[(1,1'-Biphenyl)-4-yloxy]-5-phenylpentanoic acid (**3**)*. The title compound was obtained from **3a** as a white solid; yield 45%, mp 142 – 146 °C. ^{1}H-NMR (500 MHz, $CDCl_3$) δ (ppm): 1.30 – 1.97 (m, 3H, CH_2*CH_2*CH_2 + COOH), 2.02 – 2.10 (m, 2H, *CH_2*CH), 2.68 – 2.72 (m, 2H, PhCH_2), 6.95 – 6.98, 7.17 – 7.20, 7.26 – 7.33, 7.40 – 7.43 and 7.50 – 7.54 (m, 14H, aromatics). HRMS ($C_{23}H_{22}O_3$-H)$^-$: calculated 345.1496, found 345.1490. Anal. Calcd for $C_{23}H_{22}O_3$: C, 79.74; H, 6.40. Found: C, 79.98; H, 6.37.

*2-[(1,1'-Biphenyl)-4-yloxy]-3-(2-fluorophenyl)propanoic acid (**7**).* The title compound was obtained from **7a** as a white solid; yield 16%, mp 122 – 124 °C. ^{1}H-NMR (300 MHz, $CDCl_3$) δ (ppm): 3.31 (dd, J_1=14.0 Hz, J_2=8.2 Hz, 1H of CH_2), 3.43 (dd, J_1=14.0 Hz, J_2=4.8 Hz, 1H of CH_2), 4.95 (dd, J_1=8.2 Hz, J_2=4.8 Hz, 1H, CH), 6.90 – 7.04, 7.06 – 7.21 and 7.23 – 7.51 (m, 13H, aromatics); HRMS ($C_{21}H_{17}FO_3$-H)$^-$: calculated 335.1089, found 335.1089. Anal. Calcd for $C_{21}H_{17}FO_3$: C, 74.99; H, 5.09. Found: C, 75.08; H, 5.37.

*2-[(1,1'-Biphenyl)-4-yloxy]-3-(4-fluorophenyl)propanoic acid (**8**)*. The title compound was obtained from **8a** as a white solid; yield 57%, mp 152 – 154 °C. ^{1}H-NMR (300 MHz, $CDCl_3$) δ (ppm): 2.90 – 3.10 (bs, 1H, COOH), 3.26 – 3.31 (m, 2H, CH_2), 4.87 (dd, J_1=7.0 Hz, J_2=5.2 Hz, 1H, CH), 6.89 – 7.03, 7.28 – 7.40 and 7.42 – 7.53 (m, 13H, aromatics). HRMS ($C_{21}H_{17}FO_3$-H)$^-$: calculated 335.1089, found 335.1086. Anal. Calcd for $C_{21}H_{17}FO_3$: C, 74.99; H, 5.09. Found: C, 75.38; H, 5.57.

*2-[(1,1'-Biphenyl)-4-yloxy]-3-(naphthalen-1-yl)propanoic acid (**10**)*. The title compound was obtained from **10a** as a white solid; yield 31%, mp 174 – 176 °C. ^{1}H-NMR (300 MHz, $CDCl_3$) δ (ppm): 3.67 (dd, J_1=14.4 Hz, J_2=8.8 Hz, 1H of CH_2), 3.87 (dd, J_1=14.4 Hz, J_2=3.7 Hz, 1H of CH_2), 5.02 (dd, J_1=8.8 Hz, J_2=3.7 Hz, 1H, CH), 6.76 – 6.85, 7.28 – 7.60, 7.73 – 7.91 and 8.13 – 8.21 (m, 16H, aromatics). HRMS ($C_{25}H_{20}O_3$-H)$^-$: calculated 367.1340, found 367.1367. Anal. Calcd for $C_{25}H_{20}O_3$: C, 81.50; H, 5.47. Found: C, 81.08; H, 5.37.

Synthesis of Ethyl 2-[(1,1'-biphenyl)-4-yloxy]-2-phenylacetate (1b). 4-Phenylphenol (2.3 mmol, 1.1 eq) was added to a solution of Na (2.3 mmol, 1.1 eq) in absolute ethanol (8 mL); after 1 h at room temperature, a solution of methyl 2-bromo-2-phenylacetate **1a** (2.1 mmol, 1 eq) in absolute ethanol (4 mL) was added dropwise. The mixture was stirred under reflux overnight. The solvent was distilled off and the residue dissolved in diethyl ether. The organic layer was washed with 2M NaOH, brine, dried over anhydrous Na_2SO_4, filtered and evaporated under reduced pressure to give a white solid that was purified by chromatography on a silica gel column (*n*-hexane/ethyl acetate, 80:20, as eluent); yield 62%. ^{1}H-NMR (300 MHz, $CDCl_3$) δ (ppm): 1.22 (t, J = 7.0 Hz, 3H, CH_3), 4.22 (q, J = 7.0 Hz, 2H, CH_2), 5.66 (s, 1H, CH), 7.01 – 7.04 and 7.30 – 7.62 (m, 14H, aromatics); GC-MS *m/z* (%): 332 (57) $[M]^+$, 259 (45), 163 (100), 152 (56), 135 (95), 107 (67).

Synthesis of 2-[(1,1'-biphenyl)-4-yloxy]-2-phenylacetic acid (1). 1M NaOH (15 mL, 24 eq) was added to a solution of **1b** (1.26 mmol, 1 eq) in THF (15 mL). The resulting mixture was stirred 5h at room temperature. The organic solvent was removed under reduced pressure, the aqueous residue was acidified with 6M HCl and then extracted with diethyl ether (three times). The collected organic portions were washed with brine, dried over anhydrous Na_2SO_4, filtered and concentrated to dryness obtaining a white solid which was purified by crystallization from *n*-hexane/$CHCl_3$; yield 49%, mp 190 – 192 °C. ^{1}H-NMR (300 MHz, $CDCl_3$) δ (ppm): 2.1 – 2.4 (bs, 1H, COOH), 5.7 (s,

1H, CH), 7.01 – 7.03 and 7.30 – 7.62 (m, 14H, aromatics). HRMS ($C_{20}H_{16}O_3$-H)$^-$: calculated 303.1027, found 303.1022. Anal. Calcd for $C_{20}H_{16}O_3$: C, 78.93; H, 5.30. Found: C, 79.08; H, 5.37.

Synthesis of Ethyl 2-[(4-bromobenzyl)oxy]-3-phenylpropanoate (4b). NaH (7.0 mmol, 2 eq) was suspended in anhydrous THF (20 mL), then ethyl 2-hydroxy-3-phenylpropanoate **4a** (4.67 mmol, 1 eq) dissolved in anhydrous THF (10 mL) was added at 0 °C. After 20 min, 4-bromobenzyl bromide (5.6 mmol, 1.2 eq) dissolved in anhydrous THF (10 mL) was added dropwise. The mixture was stirred under inert atmosphere at reflux overnight. Then, THF was distilled off and the residue was treated with H_2O and extracted with diethyl ether (three times). The collected organic portions were washed brine, dried over anhydrous Na_2SO_4, filtered and evaporated under reduced pressure. The resulting crude product was purified by chromatography on a silica gel column (eluent *n*-hexane/ethyl acetate, 95:5) obtaining a yellow oil; yield 28%. ^{1}H-NMR (300 MHz, $CDCl_3$) δ (ppm): 1.24 (t, J = 7.1 Hz, 3H, CH_3), 2.96 – 3.14 (m, 2H, Ph*CH*$_2$CH), 4.08 (dd, J_1 = 8.4, J_2 = 4.9 Hz, 1H, CH), 4.19 (q, J = 7.1 Hz, 2H, *CH*$_2$CH$_3$), 4.26 – 4.34 and 4.57 – 4.66 (m, 2H, OCH$_2$Ph), 6.98 – 7.11 and 7.20 – 7.49 (m, 9H, aromatics); GC-MS *m/z* (%): 365 (1) $[M+2]^+$, 363 (1) $[M]^+$, 171 (98) 169 (100), 91 (45).

Synthesis of Ethyl 2-[(1,1'-biphenyl)-4-ylmethoxy]-3-phenylpropanoate (4c). Phenylboronic acid (1.26 mmol, 2 eq), Cs_2CO_3 (0.95 mmol, 1.5 eq) and water (1 mL) were added, under a N_2 atmosphere, to a stirred solution of **4b** (0.63 mmol, 1 eq) in anhydrous toluene (15 mL); after 30 minutes at room temperature, $Pd(PPh_3)_4$ (0.032 mmol, 0.05 eq) was added. The reaction mixture was stirred at reflux 3 h and at room temperature overnight. Then, the reaction was quenched with 1M HCl and ethyl acetate (10 mL, 1:1). The suspension was filtered through a Celite pad to remove the catalyst, and the filtrate was concentrated to dryness. The residue was dissolved in ethyl acetate and washed with a saturated solution of $NaHCO_3$ (three times) and brine (three times), dried over anhydrous Na_2SO_4, filtered and concentrated to dryness obtaining a yellow oil. The crude oil was

purified by chromatography on a silica gel column (*n*-hexane/ethyl acetate, 90:10 as eluent) to give a white solid; yield 53%. ^{1}H-NMR (300 MHz, $CDCl_3$) δ (ppm): 1.24 (t, J = 7.0 Hz, 3H, CH_3), 3.01 – 3.11 (m, 2H, Ph*CH*$_2$CH), 4.11 – 4.24 (m, 3H, CH + *CH*$_2$CH$_3$), 4.37 – 4.45 and 4.66 – 4.74 (m, 2H, OCH_2Ph), 7.18 – 7.61 (m, 14H, aromatics); GC-MS *m/z* (%): 360 (1) $[M]^+$, 167 (100), 103 (19), 91 (17).

Synthesis of Ethyl 2-[(1,1'-biphenyl)-4-ylmethoxy]-3-phenylpropanoate (4). 1M NaOH (5 mL, 15 eq) was added to a solution of **4c** (0.33 mmol, 1 eq) in THF (5 mL). The resulting mixture was stirred at room temperature for 5 h. The organic solvent was removed under reduced pressure, the aqueous residue was acidified with 6M HCl and then extracted with ethyl acetate (three times). The collected organic portions were washed with brine, dried over anhydrous Na_2SO_4, filtered and concentrated to dryness obtaining a white solid, which was purified by crystallization from *n*-hexane/$CHCl_3$; yield 34%, mp 118 – 119 °C. ^{1}H-NMR (300 MHz, $CDCl_3$) δ (ppm): 3.05 (dd, J_1 = 14.0, J_2 = 7.6 Hz, 1H of Ph*CH*$_2$CH), 3.21 (dd, J_1 = 14.0, J_2 = 4.0 Hz, 1H of Ph*CH*$_2$CH), 4.08 (dd, J_1 = 7.6, J_2 = 4.0 Hz, 1H, CH), 4.46 – 4.50 and 4.61 – 4.65 (m, 2H, OCH_2Ph), 7.20 – 7.61 (m, 14H, aromatics); HRMS $(C_{22}H_{20}O_3\text{-}H)^-$: calculated 331.1340, found 331.1330. Anal. Calcd for $C_{22}H_{20}O_3$: C, 79.50; H, 6.06. Found: C, 79.08; H, 6.36.

Synthesis of Diethyl 2-benzylmalonate (5a). To a solution of diethyl malonate (4.0 mmol, 1 eq) in anhydrous DMF (2 mL), NaH (4.8 mmol, 1.2 eq) was added at 0 °C and the mixture was left at room temperature for 40 min. Then, benzyl bromide (4.8 mmol, 1.2 eq) dissolved in anhydrous DMF (1 mL) was added dropwise. The reaction mixture was stirred under inert atmosphere at room temperature overnight. Then, the mixture was diluted with water and extracted with ethyl acetate (three times). The collected organic portions were washed with brine, dried over anhydrous Na_2SO_4, filtered and evaporated under reduced pressure. The resulting crude product was purified by chromatography on a silica gel column (eluent *n*-hexane/ethyl acetate, 10:1) to obtain a colorless oil; yield 42%. ^{1}H-NMR (300 MHz, $CDCl_3$) δ (ppm): 1.24 (t, J = 7.0 Hz, 6H, 2CH_3), 3.21 (d, J=7.8

Hz, 2H, CH_2Ph), 3.61 (t, J=7.8 Hz, CH), 4.11 (q, J = 7.0 Hz, 4H, $2OCH_2$), 7.16 – 7.31 (m, 5H, aromatics); GC-MS *m/z* (%): 250 (46) $[M]^+$, 176 (46), 159 (35), 131 (100), 91 (41).

Synthesis of 2-Benzylpropane-1,3-diol (5b). To a solution of $LiAlH_4$ (6.72 mmol, 4 eq) in anhydrous THF (10 mL), **5a** (1.68 mmol, 1 eq) dissolved in anhydrous THF (5 mL) was slowly added dropwise at 0 °C under inert atmosphere. The reaction mixture was left at room temperature for 3h. Then, the mixture was cooled to 0 °C and quenched with 1 mL of water, 0.5 mL of 15% NaOH and finally 1 mL of water. The reaction mixture was filtered on a Gooch funnel and washed with ethyl acetate; the resulting filtrate was concentrated under reduced pressure obtaining a yellow oil that was purified by chromatography on a silica gel column, (ethyl acetate/n-hexane 90:10 as eluent) to give a colorless oil; yield 72%.[60] ^{1}H-NMR (300 MHz, $CDCl_3$) δ (ppm): 2.01 – 2.08 (m, 1H, CH), 2.09 – 2.27 (bs, 2H, 2OH), 2.61 (d, J=7.6 Hz, 2H, $PhCH_2$), 3.66 (dd, J_1=10 Hz, J_2=6.9, 2H, CH_2O), 3.79 (dd, J_1=10 Hz, J_2=4.1, 2H, CH_2O), 7.17 – 7.28 (m, 5H, aromatics); ESI-MS *m/z*: (IP: positive) 167 $[M+H]^+$.

Synthesis of 3-[(1,1'-Biphenyl)-4-yloxy]-2-benzylpropan-1-ol (5c). A solution of diisopropylazodicarboxylate (DIAD, 1.20 mmol, 1 eq) in anhydrous toluene (5 mL) was added dropwise to an ice-bath cooled mixture of **5b** (1.20 mmol, 1 eq), 4-phenylphenol (1.20 mmol, 1 eq), and triphenylphosphine (1.20 mmol, 1 eq) in anhydrous toluene (5 mL). The reaction mixture was stirred at room temperature overnight under inert atmosphere. The solvent was evaporated *in vacuo*, and the residue was purified by chromatography on a silica gel column (*n*-hexane/ethyl acetate 80:20 as eluent) to afford the desired compound as a white solid; yield 44%. ^{1}H-NMR (300 MHz, $CDCl_3$) δ (ppm): 2.33 – 2.36 (m, 1H, CH), 2.81 (d, J=7.6 Hz, 2H, CH_2Ph), 3.71 – 3.87 (m, 2H, CH_2OH), 3.94 – 4.13 (m, 2H, CH_2O), 6.92 – 7.00 and 7.16 – 7.59 (m, 14H, aromatics); GC-MS *m/z* (%): 318 (28) $[M]^+$, 170 (100), 91 (31), 115 (12).

Synthesis of 3-[(1,1'-Biphenyl)-4-yloxy]-2-benzylpropanoic acid (5). A solution of **5c** (0.513 mmol) dissolved in ethyl acetate (6 mL) was added dropwise to a biphasic mixture of 10% w/v aqueous $NaIO_4$ (30 mL) and ethyl acetate (15 mL). The reaction mixture was stirred mechanically using a teflon stirrer blade supporting $RuO_2 \cdot H_2O$ as a catalyst and left at room temperature for 24h.[24] The mixture was treated with ethyl acetate, water and brine, then the aqueous layer was extracted with CH_2Cl_2 (three times), and the collected organic portions were washed with brine, dried over anhydrous Na_2SO_4, filtered and evaporated under reduced pressure to give a crude solid which was purified by chromatography on a silica gel column (*n*-hexane/ethyl acetate 80:20 as eluent). The pure final compound was obtained by crystallization from *n*-hexane/$CHCl_3$ as a white solid; yield 18%, mp 163 – 165 °C. ^{1}H-NMR (300 MHz, $CDCl_3$) δ (ppm): 1.36 – 2.15 (bs, 1H, COOH), 2.96 – 3.08 (m, 1H, CH), 3.12 – 3.25 (m, 2H, $PhCH_2$), 4.05 – 4.21 (m, 2H, OCH_2), 6.87 – 6.99 and 7.19 – 7.60 (m, 14H, aromatics); HRMS $(C_{22}H_{20}O_3\text{-}H)^-$: calculated 331.1340, found 331.1331. Anal. Calcd for $C_{22}H_{20}O_3$: C, 79.50; H, 6.06. Found: C, 79.18; H, 6.46.

Synthesis of 2-(4-Phenylphenoxy)-2-methyl-3-phenylpropanoic acid (6). NaOH (powder, 10 mmol, 5 eq) and phenylacetone (0.53 mL, 3 eq) were added to a solution of 4-phenylphenol (2 mmol, 1 eq) in THF (15 mL) at 0 °C. After 0.5 h at room temperature, $CHCl_3$ (0.8 mL, 5 eq) was added dropwise during 1 h. The resulting mixture was stirred at room temperature overnight, after which the organic solvent was distilled off and the dark solid residue was treated with H_2O and washed with diethyl ether. The aqueous layer was acidified with 2M HCl up to pH = 1 and then extracted with ethyl acetate. The organic phase was extracted with $NaHCO_3$ saturated solution. The aqueous phase was carefully acidified with 6M HCl and extracted four times with ethyl acetate, washed with brine, dried over Na_2SO_4, filtered, and evaporated to dryness. The resulting crude product was crystallized from $CHCl_3$/*n*-hexane affording a white solid; yield 35%, mp = 149–150 °C; 1H-NMR (500 MHz, CD_3OD) δ (ppm): 1.40 (s, 3H, CH_3), 3.19 and 3.35 (2d, 2H, CH_2, J = 13.2 Hz), 6.94–6.97, 7.22–7.31, 7.36–7.40 and 7.48–7.56 (m, 14H, aromatics); HRMS $(C_{22}H_{20}O_3\text{-}H)^-$:

calculated 331.1340, found: 331.1335. Anal. Calcd for $C_{22}H_{20}O_3$: C, 79.50; H, 6.06. Found: C, 79.29; H, 6.39.

Synthesis of Ethyl 2-[(1,1'-biphenyl)-4-yloxy]acetate (9a). Sodium ethoxide was prepared dissolving Na (1.696 mmol, 1 eq) in absolute ethanol (5 mL), then 4-phenylphenol (1.696 mmol, 1 eq) was added and the solution was stirred for 30 minutes. Then, a solution of ethyl bromoacetate (1.696 mmol, 1 eq) in absolute ethanol (5 mL) was added dropwise and the reaction mixture was refluxed for 24 h. The solvent was removed in vacuo and the resulting crude product was treated with water and acidified with 2M HCl. The aqueous layer was extracted with diethyl ether (three times). The organic portions were collected and washed with brine, dried over anhydrous Na_2SO_4, filtered and concentrated to dryness. The crude residue was purified by column chromatography on silica gel column (eluent *n*-hexane/ethyl acetate 80:20) obtaining a white solid; yield 57%. ^{1}H-NMR (300 MHz, $CDCl_3$) δ (ppm): 1.31 (t, J = 7.0 Hz, 3H, CH_3), 4.29 (q, J = 7.0 Hz, 2H, CH_2CH_3), 4.66 (s, 2H, OCH_2), 6.97 – 7.00 (m, 2H, aromatics), 7.26 – 7.33 (m, 1H, aromatic), 7.39 – 7.44 (m, 2H, aromatics), 7.51 – 7.56 (m, 4H, aromatics); GC-MS *m/z* (%): 256 (100) $[M]^+$, 169 (49), 152 (62), 141 (24).

Synthesis of Ethyl 2-[(1,1'-biphenyl)-4-yloxy]-3-phenyl-3-[(phenylsulfonyl)oxy]propanoate (9b). n-Butyllithium (2M in hexane, 0.82 mL, 1.64 mmol) was added to a solution of 0.24 mL (1.71 mmol) of diisopropylamine in 2 mL of anhydrous THF at -78 ° C under inert atmosphere. After 30 minutes, **9a** (1.37 mmol, 1 eq) dissolved in anhydrous THF (1 mL) was added dropwise. The reaction was left for 20 minutes at -78 ° C. Then, at the temperature of -30 °C, benzaldehyde (1.2 mmol, 0.88 eq) dissolved in anhydrous THF (1 mL) was added dropwise followed from benzenesulfonyl chloride (0.2 mL). The reaction mixture was left at room temperature overnight. Then, it was treated with brine and extracted twice with ethyl acetate. The combined organic phases

were dried over anhydrous Na_2SO_4, filtered and concentrated to dryness obtaining a brown oil which underwent next step without further purification.

Synthesis of (Z)-Ethyl 2-[(1,1'-biphenyl)-4-yloxy]-3-phenylacrylate (9c). **9b** (1.18 mmol) was dissolved in 3 mL of triethylamine and the reaction mixture was left under reflux for 8 hours and overnight at room temperature. Then, the mixture was acidified with 2M HCl and extracted twice with ethyl acetate. The collected organic phases were washed with brine, dried over anhydrous Na_2SO_4, filtered and concentrated to dryness to obtain a brown oil. The crude residue was purified by chromatography on silica gel column (*n*-hexane/ethyl acetate 95: 5 as eluent) to give a brown oil; yield 40%. ^{1}H-NMR (300 MHz, DMSO-d_6) δ (ppm): 1.15 (t, J = 6 Hz, 3H, CH_3), 4.18 (q, 2H, CH_2), 7.03 – 7.08, 7.28 – 7.44, 7.58 – 7.63 and 7.70 – 7.76 (m, 15H, aromatics + vinylic CH); GC-MS *m/z* (%): 344 (100) $[M]^+$, 170 (58), 152 (32).

Synthesis of (Z)-2-[(1,1'-Biphenyl)-4-yloxy]-3-phenylacrylic acid (9). 3M NaOH (5 mL, 30 eq) was added to a solution of **9c** (0.5 mmol, 1 eq) in ethanol (5 mL). The resulting mixture was stirred under reflux for 2 h. Then, the organic solvent was removed under reduced pressure, the aqueous residue was acidified with 3M HCl and then extracted with ethyl acetate. The collected organic portions were washed with brine, dried over anhydrous Na_2SO_4, filtered and concentrated to dryness. The residue was crystallized from ethyl acetate/*n*-hexane to give a white solid; yield 27%, mp 111 – 115 °C. ^{1}H-NMR (500 MHz, DMSO-d_6) δ (ppm): 7.03 – 7.05, 7.29 – 7.43, 7.58 – 7.61 and 7.70 – 7.72 (m, 15H, aromatics + vinylic CH), 13.20 – 13.40 (bs, 1H, COOH); HRMS $(C_{21}H_{16}O_3\text{-}H)^-$: calculated 315.1027, found 315.1053. Anal. Calcd for $C_{21}H_{16}O_3$: C, 79.73; H, 5.10. Found: C, 79.38; H, 5.36.

General Procedure for the Synthesis of 11 and 12. To a solution of LT175 (1.1 mmol, 1 eq) in CH_2Cl_2 (24 mL), dimethylaminopyridine (DMAP, 1.65 mmol, 1.5 eq), *N*-(3-dimethylaminopropyl)-

N'-ethylcarbodiimide hydrochloride (EDCI, 1.65, 1.5 eq) and the appropriate sulfonamide (1.1 mmol, 1 eq) were added at 0 °C. The reaction mixture was left at room temperature for 46 h. Then, CH_2Cl_2 was added and the organic phase was washed with an aqueous solution of citric acid at 10% (3 times) and brine. The organic layer was dried over anhydrous Na_2SO_4, filtered and evaporated under reduced pressure to obtain a solid which was purified by chromatography on silica gel column (eluent CH_2Cl_2/*n*-hexane 90:10), to give the desired product.

*(S)-2-[(1,1'-Biphenyl)-4-yloxy]-N-(methylsulfonyl)-3-phenylpropanamide (**11**).*The title compound was obtained from methanesulfonamide as a white solid; yield 16%, mp 54.5 – 58 °C. ^{1}H-NMR (300 MHz, $CDCl_3$) δ (ppm): 3.09 (s, 3H, CH_3), 3.23-3.29 (m, 2H, CH_2), 4.97-5.00 (m, 1H, CH), 6.93-7.60 (m, 14H, aromatics), 8.51 (s, 1H, NH); ESI-MS *m/z*: (IP: negative) 394 $[M-H]^-$; (IP: positive) 418 $[M+Na]^+$. Anal. Calcd for $C_{22}H_{21}NO_4S$: C, 66.82; H, 5.35; N, 3.54. Found: C, 67.08; H, 5.36; N, 3.89.

*(S)-2-[(1,1'-Biphenyl)-4-yloxy]-3-phenyl-N-tosylpropanamide (**12**).* The title compound was obtained from *p*-toluenesulfonamide as a white solid; yield 25%, mp 74.3 – 75.5 °C, $[\alpha]_D$: -24.8. ^{1}H-NMR (300 MHz, $CDCl_3$) δ (ppm): 2.44 (s, 3H, CH_3), 3.10 - 3.25 (m, 2H, CH_2), 4.12 (dd, J_1 = 14.3, J_2 = 7.3 Hz, 1H, CH), 6.81-7.83 (m, 18H, aromatics), 8.61 (s, 1H, NH); ESI-MS *m/z*: (IP: negative) 470 $[M-H]^-$; (IP: positive) 494 $[M+Na]^+$. Anal. Calcd for $C_{28}H_{25}NO_4S$: C, 71.32; H, 5.34; N, 2.97. Found: C, 71.08; H, 5.56; N, 3.03.

Synthesis of (S)-2-[(1,1'-Biphenyl)-4-yloxy]-N,3-diphenylpropanamide (15). LT175 (0.314 mmol, 1 eq) was solubilized in 2 mL of $SOCl_2$ and the mixture was left under reflux for 5 h. Then, the solvent was distilled off and the residue was dissolved in anhydrous THF (2 mL). A solution of aniline (0.86 mmol, 3 eq) in anhydrous THF (1 mL) was added at 0 °C and the reaction mixture was stirred under reflux for 2 h and overnight at room temperature. Then, a saturated solution of NH_4Cl

(5 mL) was added and the mixture was acidified with 2M HCl and extracted with ethyl acetate twice. The collected organic portions were washed with brine, dried over anhydrous Na_2SO_4, filtered and concentrated to dryness to obtain a yellow solid which was crystallized from $CHCl_3$/*n*-hexane to give the desired product as a white solid; yield 45%, mp 158.6 – 160.1 °C, $[\alpha]_D$: -48.4 (c 0.25, $CHCl_3$). ^{1}H-NMR: (300 MHz, $CDCl_3$) δ (ppm): 3.29 (dd, J_1 = 14.2, J_2 = 7.0 Hz, 1H of CH_2), 3.42 (dd, J_1 = 14.2, J_2 = 3.9 Hz, 1H of CH_2), 4.93 (dd, J_1 = 7.0, J_2 = 3.9 Hz, 1H, CH); 6.92-7.55 (m, 19H, aromatics); 7.94 (s, 1H, NH); GC/MS *m/z* (%): 393 (32.3) $[M]^+$, 224 (56), 170 (100). Anal. Calcd for $C_{27}H_{23}NO_2$: C, 82.42; H, 5.89; N, 3.56. Found: C, 82.08; H, 6.30; N, 4.00.

Synthesis of (S)-2-[(1,1'-Biphenyl)-4-yloxy]-3-phenylpropanamide (17). LT175 (0.63 mmol) was dissolved in 2 mL of $SOCl_2$ and the mixture was left under reflux for 2 h. Then, the solvent was distilled off and the residue was dissolved in anhydrous THF (2 mL). A 30% ammonium hydroxide solution (2 mL) was added at 0 °C and the reaction mixture was stirred at room temperature overnight. Then, a saturated solution of NH_4Cl (5 mL) was added to the mixture which was extracted with ethyl acetate twice. The collected organic portions were washed with brine, dried over anhydrous Na_2SO_4, filtered and concentrated to dryness to obtain a white solid; yield 78%. ^{1}H-NMR (500 MHz, $CDCl_3$) δ (ppm): 3.23 (dd, J_1 = 14.3, J_2 = 7.3 Hz, 1H of CH_2), 3.35 (dd, J_1 = 14.3, J_2 = 3.7 Hz, 1H of CH_2), 4.82 (dd, J_1 = 7.3, J_2 = 3.7 Hz, 1H, CH); 5.50 (s, 1H of NH_2); 6.25 (s, 1H of NH_2); 6.93 – 6.98, 7.21 – 7.36, 3.39 – 7.44 and 7.47 – 7.54 (m, 14H, aromatics); GC/MS *m/z* (%): 317 (31.1) $[M]^+$, 170 (100), 105 (34).

Synthesis of (S)-2-[(1,1'-Biphenyl)-4-yloxy]-3-phenylpropan-1-amine (18). **13a** (0.49 mmol, 1 eq) was dissolved in anhydrous THF (10 mL) under inert atmosphere. Then, 1M $BH_3 \cdot$ THF (1.5 mL, 3 eq) was added dropwise and the reaction mixture was left under reflux for 3 h. Then, the reaction was quenched with 7 mL of MeOH and left under stirring for about 5 minutes; the solvent was concentrated to dryness to obtain a brown oil; yield 90%. ^{1}H-NMR (300 MHz, $CDCl_3$) δ (ppm):

2.79-3.14 (m, 4H, $PhCH_2$ + NH_2), 3.53-3.75 (m, 2H, CH_2N), 4.41-4.53 (m, 1H, CH), 6.94 – 7.02 and 7.20 - 7.59 ppm (m, 14H, aromatics); GC/MS m/z (%): 303 (13.6) $[M]^+$, 170 (100), 134 (86.3), 91 (78.4).

General Procedure for The Synthesis of 13 and 14. 13b (0.59 mmol, 1.2 eq) was dissolved in anhydrous THF (7 mL) under inert atmosphere. Triethylamine (0.98 mmol, 2 eq) and the suitable sulfonyl chloride (0.49 mmol, 1 eq), previously dissolved in 1 mL of anhydrous THF, were added at 0 °C. The reaction mixture was stirred at 0 °C for 2 h. Then, it was quenched with water, acidified with 2M HCl and extracted twice with ethyl acetate. The collected organic portions were washed with brine, dried over anhydrous Na_2SO_4, filtered and concentrated to dryness obtaining a yellow oil which was purified by chromatography on silica gel column (eluent CH_2Cl_2) to give a colorless oil. The desired product was obtained by crystallization from $CHCl_3$/*n*-hexane.

*(S)-N-{2-[(1,1'-Biphenyl)-4-yloxy]-3-phenylpropyl}methanesulfonamide (**13**).* The title compound was obtained from methanesulfonyl chloride as a white solid; yield 19%, mp 108.1 – 109.7 °C, $[\alpha]_D$: -27.6 (c 0.5, CH_3OH). ^{1}H-NMR (300 MHz, $CDCl_3$) δ (ppm): 1.65 (s, 3H, CH_3), 2.92-3.17 (m, 2H, $PhCH_2$); 3.25-3.47 (m, 2H, CH_2N), 4.64-4.71 (m, 2H, CH+NH), 6.98 – 7.03 and 7.23 - 7.60 (m, 14H, aromatics); GC/MS *m/z* (%): 381 (16.8) $[M]^+$, 170 (100), 108 (24.8). Anal. Calcd for $C_{22}H_{23}NO_3S$: C, 69.26; H, 6.08; N, 3.67. Found: C, 69.08; H, 6.36; N, 4.10.

*(S)-N-{2-[(1,1'-Biphenyl)-4-yloxy]-3-phenylpropyl}benzenesulfonamide (**14**).* The title compound was obtained from benzenesulfonyl chloride as a white solid; yield 8%, mp 106.7 – 107.6 °C, $[\alpha]_D$: -43.2 (c 0.25, CH_3OH). ^{1}H-NMR (300 MHz, $CDCl_3$) δ (ppm): 2.81-3.32 (m, 4H, $PhCH_2$ + CH_2N), 4.36-4.56 (m, 1H, CH), 4.79 – 4.89 (m, 1H, NH), 6.84 – 6.88, 7.14 – 7.59 and 7.76 - 7.79 (m, 19H, aromatics); GC/MS *m/z* (%): 443 (13.6) $[M]^+$, 170 (100), 141 (21.4); HRMS $(C_{27}H_{25}NO_3S\text{-}H)^-$:

calculated 442.1482, found 442.1468. Anal. Calcd for $C_{27}H_{25}NO_3S$: C, 73.11; H, 5.68; N, 3.16. Found: C, 72.88; H, 5.36; N, 3.51.

Computational Chemistry

Protein and Ligand Preparation. The crystal structures of PPARα in complex with AL29-26 (PDB 5HYK)[32] and PPARγ in complex with the LT175 (PDB 3B3K)[18] were fetched from the Protein Data Bank (PDB). These structures were selected for docking calculations because of their completeness, good resolution and the similarity of the co-crystallized ligands AL29-26 and LT175 bulky aromatic scaffolds with this series of derivatives. In fact, in both crystal structures the ligand-induced switching of F273 (for PPARα) and F282 (for PPARγ) side chains to the open conformation occurred, allowing the accommodation of rigid and straight substituents at the carbon atom linked to the carboxylate group. The two crystal structures were preprocessed and optimized with the Protein Preparation Wizard in Maestro (Protein Preparation Wizard; Epik, Schrödinger, LLC, New York, NY, 2021; Impact, Schrödinger, LLC, New York, NY; Prime, Schrödinger, LLC, New York, NY, 2021). All the crystallographic water molecules and other chemical components were removed, the right bond orders, charges and atom types were assigned, and the hydrogen atoms were added. The H-bond network was optimized by exhaustive sampling of rotamers, tautomers and protonation states of titratable amino acids at neutral pH. The imidazole rings of H440 into PPARα, H449 and H323 into PPARγ were set in their Nε 2-H (N tau-H) tautomeric state. Finally, a restrained minimization was performed on the protein structures using the Impref module with the OPLS4 force field, by imposing a 0.3 Å RMSD limit from the initial coordinates as constraint. The investigated compounds were created with Maestro 2D-sketcher and prepared with LigPrep (LigPrep, Schrödinger, LLC, New York, NY, 2021) to generate suitable 3D conformations and tautomerization states at pH 7.0 ± 2.0. The compounds were then energetically minimized using the OPLS4 force field, and the resulting 3D structures used to specify chiral centers.

Docking Simulations. Docking of compounds under study was performed with the Glide algorithm in Extra Precision (XP) mode.[61,62] For the docking grid generation, an inner box of 20 Å X 20 Å X 20 Å, surrounding each ligand binding cavity site was considered. A scaling factor of 0.8 was set for van der Waals radii of receptor atoms. Ligand sampling was allowed to be flexible. Default docking parameters were used, and no constraints were included. The Glide XP GScore and Emodel functions were used to score and rank the predicted binding poses. To remove any residual geometric strain, the obtained complexes were energy-minimized by means of MacroModel (MacroModel, Schrödinger, LLC, New York, NY, 2021), using the OPLS4 force field with steepest descent (100 iterations) followed by Polak-Ribiere conjugate gradient methods (5000 iterations). Upon minimization, the protein backbone atoms were held fixed. All the figures were rendered with PyMOL (The PyMOL Molecular Graphics System, Version 2.0 Schrödinger, LLC).

Biological Experiments

PPAR Assay. Reference compounds, the cell culture medium and other reagents were purchased from Sigma-Aldrich (Milan, Italy). The expression vectors bearing the chimeric receptor containing the yeast Gal4-DNA binding domain fused to the human PPARα- or PPARγ-LBD, and the reporter plasmid for these Gal4 chimeric receptors (pGal5TKpGL3), comprising five repeats of the Gal4 response elements upstream of a minimal thymidine kinase promoter adjacent to the coding sequence for luciferase, were described in a previous work.[27] A culture of the human hepatoblastoma cell line HepG2 (Interlab Cell Line Collection, Genoa, Italy) was conducted in minimum essential medium (MEM) containing 10% heat-inactivated fetal bovine serum, 100 U of penicillin G mL^{-1}, and 100 μg of streptomycin sulfate mL^{-1} at 37 °C in a humidified atmosphere of 5% CO_2. For transactivation assays, cells were seeded in a 24-well plate at a concentration of 10^5 cells per well, and were transfected after 24 h with CAPHOS, a calcium phosphate method,

according to the manufacturer's guidelines. Cell transfection was performed using expression plasmids encoding the fusion protein Gal4-PPARα-LBD or Gal4-PPARγ-LBD (30 ng), pGal5TKpGL3 (100 ng), and pCMVβgal (250 ng). Following transfection, cells were incubated for 4 h, after which they underwent treatment with the indicated ligands in triplicate for 20 h. Cell extracts were subsequently analyzed for luciferase activity via luminometry (VICTOR^3 V multilabel plate reader, PerkinElmer). Ortho-nitrophenyl-β-D-galactopyranoside was used to measure β-Galactosidase activity, following a previously described method.[63] All transfection experiments were performed at least twice.

*In Vivo Pharmacokinetic Study of Compound **10***

Chemicals and Reagents. MS grade (≥ 99.0% pure) ammonium formate and formic acid were sourced from Sigma Aldrich. HPLC grade acetonitrile, methanol, isopropyl alcohol and dimethyl sulfoxide solvents were purchased from Merck Germany. Milli-Q® Water used for the preparation of mobile phase, rinsing solvent and seal washes was obtained from the in-house (Eurofins Advinus limited) Milli-Q® system. The internal standard Warfarin ($C_{19}H_{16}O_4$, 308.33, purity ≥ 97%) used in the study was procured from Sigma Aldrich. Male Sprague-Dawley rats (220 – 240 g) were obtained from HyLasco Biotechnology (India) Pvt. Ltd. (Subsidiary of Charles River from US). A SCIEX API 6500+™ LC/MS/MS triple quadrupole mass spectrometer system equipped with a negative Electrospray ionization (ESI) source and Shimadzu prominence HPLC comprising of binary pumps, column oven and SIL-HTC autosampler was used in the study. Data acquisition, integration and quantification were performed using Analyst® 1.6.3.

Chromatographic and Mass Spectrometric Conditions. Liquid chromatographic separations of compound **10** and internal standard, Warfarin, were achieved on a reverse phase Kinetex EVO C18, 100 x 4.6 mm, 2.6 µm column operating at 40 °C. The isocratic mobile phase was a 20:80 (v/v)

mixture of 10 mM ammonium formate containing 0.1% formic acid (Mobile phase A) and 0.1% formic acid in acetonitrile (Mobile phase B) delivered at a flow rate of 0.8 mL/min without splitter. Mass spectrometer was operated in negative electrospray ionization mode with unit mass resolution in a quadrupole analyzer with 200 ms dwell time and the analytes were detected by multiple reaction monitoring (MRM). The compound parameters of **10** and Warfarin (internal standard) were optimized along with the MRM transition (m/z) to achieve sensitivity. Source parameters were optimized to a curtain gas N_2 flow of 30 psi (CUR), nebulizer N_2 gas of 40 psi (gas 1), ion spray voltage of -4500 V (IS), auxiliary N_2 gas of 50 psi (gas 2) with turbo spray temperature of 550 °C (TEMP) and collision-activated dissociation gas (CAD) of 8 psi. MRM transition (m/z) selected for the analyte **10** was 367.1 → 169.1 and Warfarin (Internal standard) was 307.1 → 160.9. System suitability test was performed prior to analysis of samples. System suitability test comprised of six replicate injections of extracted ULOQ and an extracted blank and LLOQ sample from rat plasma. The percentage coefficient of variation (CV (%)) for peak area ratio (analyte to internal standard) of six replicate injections was ≤ 5%, which met the acceptance criteria. The retention time was within ±0.5 min variation in each analytical run. *Sample Preparation.* Extraction of **10** and Warfarin (Internal standard) from samples of rat plasma was done by a protein precipitation (crashing) method. To 20 µL aliquot of CC/QC/Study samples, 20 µL of Internal Standard Working Solution were added to all the tubes except for Standard Blank sample and vortexed. To the Standard Blank sample 20 µL of diluent were added. To all the pre-labelled microcentrifuge tubes (1.5 mL capacity), 0.20 mL of acetonitrile were added for precipitation and vortexed (Vibramax 100, Heidolph Instruments) for about 10 min. The above samples were centrifuge (Eppendorf 5810R) for 10 min at 10000 rpm and 4 °C. About 10 µL of the supernatant sample was injected for analysis into SCIEX API 6500+ LC-MS/MS system.

Preparation of Calibration Standards and Quality Control Samples. The stock solutions of **10** and warfarin (internal standard) were prepared in dimethylsulphoxide (DMSO) and acetonitrile at 1

mg/mL concentration, respectively. The stock solution of **10** was further diluted using DMSO to prepare calibration standard solutions in the concentration range of 20 to 40000 ng/mL. For internal standard, acetonitrile was used to prepare a working solution of concentration 500 ng/mL. These solutions were then spiked in interference-free rat blank plasma to obtain calibration standards in the pharmacologically relevant range (1 to 2000 ng/mL). Similarly, the quality control (QC) samples were prepared using independent stock solutions of analytes to obtain the concentrations of 4.00, 400 and 1000 ng/mL in rat plasma, representing low, medium and high concentration QC samples, respectively. The stock solutions, diluted standard solutions, quality control solutions and internal standard solution were stored at 2–8 °C. The spiked plasma samples (calibration standards and quality controls) were prepared freshly prior to sample analysis.

*Bioavailability Study of **10** in Male Sprague-Dawley Rats.* Sprague-Dawley rats for the study were obtained from HyLasco Biotechnology (India) Pvt. Ltd. (Subsidiary of Charles River from US). Animals were housed in polysulfonate cages with an enrichment device under typical research laboratory environments (temperature 25 ± 3 °C, relative humidity 50% to 70%), with an approximately 12 h light/dark cycle. Altromin Rat/Mice maintenance diets manufactured by Altromin Spezialfutter GmbH, Germany and charcoal filtered water after UV ray's treatment were used during the study. Experimentation on animals were approved by the Institutional Animal Ethics Committee and were in accordance with the Committee for the Purpose of Control and Supervision of Experiments on Animals (CPCSEA), Ministry of Social Justice and Environment, Government of India. All the rats were jugular vein cannulated and overnight fasted prior to dosing (except IV dose), and approximately 4 h post dose food was offered to all animals. Formulations were made prior to dosing with test compound **10** and were maintained on continuous stirring during dosing. Compound **10** in 10% DMSO + pH 7.4 PBS was used for IV administration, whereas **10** in 10% DMSO + 5% Cremophor EL + 30% PEG400 + 20% PG + pH 7.4 PBS was used for PO administration. Animal weight on the day of dosing was used to calculate the required

volume of formulation, which was administered to the rats accordingly. Test compound **10** at a dose of 1 mg/kg body weight was injected as intravenous bolus and at a dose of 5 mg/kg body weight administered orally. Blood samples at a volume of approximately 0.250 mL were collected from the jugular vein at 0.083 (IV only), 0.25, 0.5, 1, 2, 4, 6, 8, and 24h post dose administration into prelabelled microcentrifuge tubes containing dipotassium ethylenediaminetetraacetic acid (K_2EDTA) anticoagulant at the final concentration of 4 mM. The blood samples, after mixing, were centrifuged at 2400 g for 10 min at a set temperature of 4 °C. The collected plasma samples were stored below –60 °C until bioanalysis. Pharmacokinetic parameters were calculated by a non-compartmental analysis tool of the validated Phoenix® WinNonlin® 8.3. $C_{max,}$ and T_{max} and exposures (AUC_{last} and $AUC_{infinity}$) were calculated as applicable. Additionally, pharmacokinetic parameters for parenteral route like C_0, elimination half-life ($T_{1/2}$), hepatic clearance (Cl), distribution volume (Vd), were estimated. Absolute oral bioavailability (%F) was calculated with dose-normalized exposure of non-intravenous against dose-normalized intravenous exposure.

In Vivo Antihyperglycemic Screening: Streptozotocin-Induced Diabetic Mice Model. Swiss Albino mice weighing about 13-34 g were used for animal studies. Experimental protocols were approved by the Institutional Animal Ethical Committee (No. 1972/PH/BIT/132/21/IAEC) of the Department of Pharmaceutical Sciences and Technology, Birla Institute of Technology, Mesra, Ranchi. All the experiments were conducted in accordance with National Institutes of Health Guide for Care and Use of Laboratory animals. Polypropylene cages containing wood shaving as bedding material were used for housing the experimental animals in 6 groups of 5 animals each. All the groups were maintained in the departmental animal house with a natural light/dark cycle at 26 ± 2 °C and 44–55% relative humidity for 7 days.[64] All animals (except normoglycemic control, Group 6) were rendered diabetic by the administration of streptozotocin in 0.1 M citrate buffer (pH 4.5) at a dose of 40 mg/kg body weight (bw) for 5 consecutive days through intraperitoneal route. Drinking water was replaced with 10% sucrose solution on days 4 and 5. Then the animals were monitored for next

12 days for the development of diabetes. Mice were considered as diabetic if their blood glucose levels were above 250 mg/dL on days 10-12 after streptozotocin administration. Normoglycemic control group received normal saline. Animals were grouped as follows: diabetic control (Group 1), mice treated with 30 mg/kg pioglitazone bw (Group 2), mice treated with 25 mg/kg bw **10** (Group 3), mice treated with 50 mg/kg bw **10** (Group 4), mice treated with 25 mg/kg bw **10** + pioglitazone (Group 5), normoglycemic control (Group 6). Groups 2, 3, 4 and 5 received standard and test drugs as 0.25% suspension in Tween 80 by oral route for 15 days. Blood glucose levels were determined from blood obtained from tail vein of the animal on Days 0, 5, 10 and 15, using glucose meter (Contour plus, Ascensia Diabetes Care Holdings AG). All animals had *ad libitum* access to food (rodent diet) and water before, during and after the experiment.

*Lipid Profiling of Compound **10** in Streptozotocin-Induced Diabetic Mice Model.* Before sacrificing the animals, blood samples were collected from retro-orbital region under light anaesthesia and were pooled group-wise for measurement of total cholesterol (TC), high-density lipoprotein cholesterol (HDL), low-density lipoprotein cholesterol (LDL), very low-density lipoprotein cholesterol (VLDL), and triglycerides (TG). All these measurements were done by using commercially available kits in a clinical analyzer.

Histopathological Study. Mice from each group were sacrificed under light anaesthesia using diethyl ether. Bone, kidney and liver tissues were dissected, washed in ice cold physiological saline, fixed in a 15% buffered neutral formalin solution and, finally, embedded into paraffin blocks. Then, the tissue was sliced out into sections of 5 μm thickness by a rotator microtome and stained with hematoxylin-eosin. Obtained sections were examined by a Leica DME microscope, and representative photomicrographs were taken by a 7.1 megapixel Canon Power Shot S70 digital camera.

Expression and Purification of Human Recombinant PTP1B. Recombinant human PTP1B (1-302 aa) was obtained in our laboratory.[65] Briefly, the nucleotide sequence of the PTP1B protein (1-303 aa) was cloned within the bacterial expression plasmid pNick28, downstream the poly-histidine tag. Once the correctness of the cloning has been verified, the plasmid was used to transform E. Coli BL21 bacterial cells previously made competent to host the plasmid. The clones that acquired the plasmid were grown on LB medium containing kanamycin antibiotic for selection. Bacterial cells harbouring plasmid were stored at -80°C. To produce the PTP1B, an aliquot of transformed bacteria was grown in larger volume of LB (1 L) upon reaching an optical density value equal to OD_{600} = 0.8 and then stimulated with isopropil-β-D-1-thiogalattopiranoside for 3 h. After this time, bacteria were collected by centrifugation and stored at -20°C. Recombinant PTP1B was separated from other bacterial proteins by liquid chromatography, using a column packed with a high-capacity HisPur Ni-NTA resin (Thermo Fisher Scientific 168 Third Avenue Waltham, MA USA). Fractions containing PTP1B were collected, concentrated using an Amicon centrifugal filter unit until a final volume of 5 mL. The sample was purified by gel filtration using a Superdex G75 column equilibrated with 50 mM Tri-HCl buffer pH 8.0, containing 150 mM NaCl and 0.5 mM β-mercaptoethanol. After chromatography, fractions containing the enzyme were collected, concentrated, divided in aliquots of about 1 mL, and stored at -80°C. The purity of preparation was determined by SDS-PAGE method.

Enzymatic Assays. PTP1B activity was determined as previously described.[66] The synthetic substrate *p*-nitrophenyl-phosphate (*p*-NPP) was dissolved in 0.075 M β-β-dimethylglutarate buffer pH 7.0 containing 0.5 mM EDTA, and 0.1 mM DTT. Reactions were started by adding an aliquot of PTP1B in the assay buffer and stopped after an appropriate time by adding 2 mL of 0.1 M KOH. The *p*-nitrophenol released in the assay buffer was determined measuring the absorbance of assay solutions at 400 nm. The IC_{50} value was determined measuring the residual activity of PTP1B in the presence of increasing inhibitor concentrations. All tests were carried out in triplicate and

data obtained were normalized respect to control sample. Experimental points were fitted using the following equation

$$\frac{V_i}{V_0} = \frac{Max - Min}{1 + \left(\frac{1}{IC_{50}}\right)^{slope}} + Min$$

where V_i and V_0 represent the enzymatic activity measured in the presence and absence of the inhibitor, respectively; Max and Min represent the maximum and minimum value of the activity; the slope represents the slope of the curve in the transition region, and the IC_{50} value represents the concentration of inhibitor capable of reducing the enzymatic activity by 50%.

Cell Cultures and Ex Vivo Assays. Murine myoblasts (C2C12) were purchased from the European Collection of Authenticated Cell Cultures (ECACC). Cells were grown in Dulbecco's Modified Eagle's medium (DMEM) supplemented with 10% foetal bovine serum (FBS), 2 mM glutamine, 100 IU/mL penicillin, 100 µg/mL streptomycin (Sigma-Aldrich, St. Louis, MO, USA), under controlled conditions (humidified atmosphere and with 5% CO_2 at 37 °C). The impact of compound **10** on the insulin-signaling pathway was evaluated by analyzing the levels of Akt phosphorylation using the western blot method. In summary, C2C12 cells were starved for 24 h and then stimulated for 30 min with 10 nM insulin, 25 µM of compound **10** or insulin-compound **10** combination. Subsequently, the cells were lysed, and the protein extracts loaded onto prefabricated 4-20% polyacrylamide gel (Biorad). Finally, the proteins were transferred to the PVDF membrane by western blot. Akt kinase phosphorylation levels were probed using specific antibodies: phospho-protein kinase B (p-Akt, 9271S) and Akt (9272S) antibodies were from Cell Signalling Technology (Danvers, Massachusetts, USA); secondary antibodies were from Santa Cruz Biotechnology Inc. (Dallas, Texas, USA). The ability of compound **10** to impair GLUT4 activity or to promote AMPK activation was evaluated by pre-treating C2C12 cells with Cytochalasin B (Sigma-Aldrich, C6762)

or Compound C (Sigma-Aldrich, 171260). Briefly, starved C2C12 cells were incubated for 1 h in the presence of Cytochalasin B or Compound C. After this time, cells were washed with PBS and stimulated with 25 mM compound **10** for 30 min. Then, cells were washed again and incubated for three hours in the presence of 40 mM 2-NBDG for 3 h. Finally, the amount of fluorescent glucose uploaded by cells was evaluated using a flow cytometer. All tests were carried out in triplicate.

Glucose Uptake Assay. Glucose uptake by C2C12 cells was determined using 2-NBDG.[67] Briefly, C2C12 cells were seeded in 24 well plates and once reached 70% confluence starved for 20 h. After this time, cells were stimulated with 10 nM insulin (Humalog Lispro, Eli Lilly), or 25 μM **10** or with a combination of **10**-insulin for 30 min. After stimulation, cells were incubated in the presence of 40 μM 2-NBDG (Invitrogen) for 3 h. Then, cells were washed with PBS, tripsinized, pelleted by centrifugation (1000xg for 5 min), and finally suspended in 500 μL of PBS. The amount of 2-NBDG uploaded by cells was determined using a flow cytometer apparatus (FACSCanto II, BD Biosciences, San Jose, CA, USA). For each samples $1x10^4$ events were acquired. Data obtained were then analyzed with FlowJo software. Cells autofluorescence values were determined before sample analysis and subtracted to each sample.

Seahorse Xfe96 Metabolic Assays. Fifteen thousand cells/well (C2C12) were seeded in XFe96 cell culture plates in complete growth medium. After 24 h, the medium was replaced with an XF base medium supplemented with 2 mM glutamine, 1 mM sodium pyruvate, and 25 mM glucose. Cells were then incubated in a non-CO_2 incubator for 1 h at 37 °C to pre-equilibrate the cells before analysis. An XF Mito Stress Test was performed to assay the cells' ability to exploit mitochondrial oxidative metabolism, according to the manufacturer's instructions.[68] Protein quantification was used to normalize the results. All tests were carried out in quadruplicate.

Determination of Mitochondrial Membrane Potential. To determine the impact of **10** on mitochondrial membrane potential, the C2C12 muscle cells were incubated in the presence or absence of 25 μM **10** for 30 min. After incubation, cells were washed with PBS and incubated in the presence of 100 nM TMRE for 30 min. Then, cells were detached and analysed using a flow cytometer. All tests were carried out in triplicate. Data obtained were normalized respect to control cells.

Determination of Cell Viability by MTT Method. MTT assay was carried out to evaluate the impact of **10** on C2C12 muscle cells viability. Briefly, C2C12 (10^4 cells/well) were grown in 24 well plates and incubated in the presence of 25 μM **10** for 48 h. After this time, cells were washed with PBS, and incubated with 400 μL of 0.5 mg/mL MTT dissolved in DMEM. Cells were stored in a CO_2 incubator for 4 h. After incubation period, growth medium was removed, cells were washed with PBS and then lysed adding 500 μL of DMSO to dissolve formazan salts generated by enzymatic complex of cells. The amount of formazan crystals generated in the culture is proportional to the number of metabolically active cells. Finally, the absorbance of samples was determined via a multimode plate reader by using a wavelength of 595 nm (Biorad 550). All data were normalized respect to control sample, which was carried out incubating muscle cells with an equivalent amount of DMSO, the solvent used to dissolve each compound.

Statistical Analysis. Data in vitro reported in this study were analyzed using Unpaired Student's T test. p values < 0.05 were considered statistically significant. (* $p < 0.05$; ** $p < 0.01$).

All statistical tests for data in vivo were performed using GraphPad Prism 5.0 software (San Diego, California, USA). Results were expressed as mean ± S.E.M. (standard error of the mean) for six rats in each group. The data was analyzed by one-way analysis of variance (ANOVA) followed by Dunnett's multiple variance test. Differences were considered statistically significant at the levels of $p < 0.05$.

Supporting Information

Biological tests on PTP1B inhibition in vitro and in cells; biological experiments ruling out the effect of Cytochalasin B and Compound C on glucose uptake induced from compound **10**; evaluation of C2C12 cell viability after acute treatment with compound **10**; HPLC trace of compound **10**. PDB files for computational models of (***S***)-**10** and (***R***)-**10** in PPARalpha and PPARgamma, respectively.

Molecular formula strings and the associated biological data (CSV).

Corresponding Authors

Antonio Lavecchia − Department of Pharmacy, "Drug Discovery" Laboratory, University of Napoli "Federico II", 80131 Napoli, Italy; orcid.org/0000-0002-2181-8026; Phone: +39-081-678613/623; E-mail: antonio.lavecchia@unina.it; Fax: +39-081-678012

Fulvio Loiodice – Department of Pharmacy-Drug Sciences, University of Bari "Aldo Moro", 70125 Bari, Italy; orcid.org/0000-0003-3384-574X; Phone: +39-080-5442778;

E-mail: fulvio.loiodice@uniba.it

Acknowledgment

This work was financially supported by the University of Bari Aldo Moro (Fondi di Ateneo 2020), University of Florence (Fondi di Ateneo 2021) and Italian Ministry of University and Research (M.U.R.). C.C. acknowledges PON R&I 2014-2020 Asse IV "Istruzione e Ricerca per il recupero - REACT-EU", Azione IV.4 - "Contratti di Ricerca su tematiche dell'Innovazione". Finally, we acknowledge dr. Judith Wackerlig and dr. Stefan Simic of Department of Pharmaceutical Sciences at the University of Vienna for supplying the HPLC chromatogram of compound **10**.

Abbreviations Used

PPAR, peroxisome proliferator-activated receptor; LBD, ligand binding domain; TZDs, thiazolidinediones; GLUT4, glucose transporter 4; PTP1B, protein tyrosine phosphatase 1B; AMPK, adenosine monophosphate-activated protein kinase; NBDG, nitrobenzofurazan-deoxy-glucose; MPC, mitochondrial pyruvate carrier.

Declaration of competing interest

The authors declare that they have no known competing financial interests.

REFERENCES

1. Yusuf, S.; Hawken, S.; Ôunpuu, S.; Dans, T.; Avezum, A.; Lanas, F.; McQueen, M.; Budaj, A.; Pais, P.; Varigos, J.; Lisheng, L. Effect of potentially modifiable risk factors associated with myocardial infarction in 52 countries (the INTERHEART study): case-control study. *Lancet* **2004**, *364*, 937–952.

2. The Emerging Risk Factors Collaboration. Major lipids, apolipoproteins, and risk of vascular disease. *JAMA* **2009**, *302*, 1993–2000.

3. Chehade, J. M.; Gladysz, M.; Mooradian, A. D. Dyslipidemia in type 2 diabetes: prevalence, pathophysiology, and management. *Drugs* **2013**, *73*, 327–339.

4. Reiner Ž. Managing the residual cardiovascular disease risk associated with HDL-cholesterol and triglycerides in statin-treated patients: a clinical update. *Nutr. Metab. Cardiovasc. Dis*. **2013**, *23*, 799–807.

5. Sosale, A.; Saboo, B.; Sosale B. Saroglitazar for the treatment of hypertriglyceridemia in patients with type 2 diabetes: current evidence. *Diabetes Metab. Syndr. Obes*. **2015**, *8*, 189–196.

6. Laganà, A. S.; Vitale, S. G.; Nigro, A.; Sofo, V.; Salmeri, F. M.; Rossetti, P.; Rapisarda, A. M. C.; La Vignera, S.; Condorelli, R. A.; Rizzo, G.; Buscema, M. Pleiotropic actions of peroxisome proliferator-activated receptors (PPARs) in dysregulated metabolic homeostasis, inflammation and cancer: current evidence and future perspectives. *Int. J. Mol. Sci.* **2016**, *17*, 999.

7. Harmon, G. S.; Lam, M. T.; Glass, C.K. PPARs and lipid ligands in inflammation and metabolism. *Chem. Rev.* **2011**, *111*, 6321–6340.

8. Zieleniak, A.; Wòjcik, M.; Woźniak, L. A. Structure and physiological functions of the human peroxisome proliferator-activated receptor γ. *Arch. Immunol. Ther. Exp.* **2008**, *56*, 331–345.

9. Neels, J. G.; Grimaldi, P. A. Physiological functions of peroxisome proliferator-activated receptor β. *Physiol. Rev.* **2014**, *94*, 795–858.

10. Hong, F.; Xu, P.; Zhai, Y. The opportunities and challenges of peroxisome proliferator-activated receptors ligands in clinical drug discovery and development. *Int. J. Mol. Sci.* **2018**, *19*, 2189.

11. Davidson, M. H.; Armani, A.; McKenney, J. M.; Jacobson, T. A. Safety considerations with fibrate therapy. *Am. J. Cardiol.* **2007**, *99*, S3-S18.

12. Yamashita, S.; Masuda, D.; Matsuzawa, Y. Pemafibrate, a new selective PPARα modulator: drug concept and its clinical applications for dyslipidemia and metabolic diseases. *Curr. Atheroscler. Rep.* **2020**, *22*, 5.

13. Bortolini, M.; Wright, M. B.; Bopst, M.; Balas, B. Examining the safety of PPAR agonists - current trends and future prospects. *Expert Opin. Drug Saf*. **2013**, *12*, 65–79.

14. Fiévet, C.; Fruchart, J. C.; Staels, B. PPARα and PPARγ dual agonists for the treatment of type 2 diabetes and the metabolic syndrome. *Curr. Opin. Pharmacol*. **2006**, *6*, 606-614.

15. Heald, M.; Cawthorne, M. A. Dual acting and pan-PPAR activators as potential anti-diabetic therapies. *Handb. Exp. Pharmacol.* **2011**, *203*, 35–51.

16. Piemontese, L.; Cerchia, C.; Laghezza, A.; Ziccardi, P.; Sblano, S.; Tortorella, P.; Iacobazzi, V.; Infantino, V.; Convertini, P.; Dal Piaz, F.; Lupo, A.; Colantuoni, V.; Lavecchia, A.; Loiodice, F. New diphenylmethane derivatives as peroxisome proliferator-activated receptor alpha/gamma dual agonists endowed with anti-proliferative effects and mitochondrial activity. *Eur. J. Med. Chem.* **2017**, *127*, 379–397.

17. Balakumar, P.; Rose, M.; Ganti, S. S.; Krishan, P.; Singh, M. PPAR dual agonists: are they opening Pandora's Box? *Pharmacol. Res.* **2007**, *56*, 91–98.

18. Montanari, R.; Saccoccia, F.; Scotti, E.; Crestani, M.; Godio, C.; Gilardi, F.; Loiodice, F.; Fracchiolla, G.; Laghezza, A.; Tortorella, P.; Lavecchia, A.; Novellino, E.; Mazza, F.; Aschi, M.; Pochetti, G. Crystal structure of the peroxisome proliferator-activated receptor gamma (PPARgamma) ligand binding domain complexed with a novel partial agonist: a new region of the hydrophobic pocket could be exploited for drug design. *J. Med. Chem.* **2008**, *51*, 7768−7776.

19. Gilardi, F.; Giudici, M.; Mitro, N.; Maschi, O.; Guerrini, U.; Rando, G.; Maggi, A.; Cermenati, G.; Laghezza, A.; Loiodice, F.; Pochetti, G.; Lavecchia, A.; Caruso, D.; De Fabiani, E.; Bamberg, K.;
Crestani, M. LT175 is a novel PPARα/γ ligand with potent insulin sensitizing effects and reduced adipogenic properties. *J. Biol. Chem*. **2014**, *289*, 6908−6920.

20. Fracchiolla, G.; Laghezza, A.; Piemontese, L.; Tortorella, P.; Mazza, F.; Montanari, R.; Pochetti, G.; Lavecchia, A.; Novellino, E.; Pierno, S.; Conte Camerino, D.; Loiodice, F. New 2-

aryloxy-3-phenylpropanoic acids as peroxisome proliferator-activated receptors alpha/gamma dual agonists with improved potency and reduced adverse effects on skeletal muscle function. *J. Med. Chem*. **2009**, *52*, 6382−6393.

21. Laghezza, A.; Pochetti, G.; Lavecchia, A.; Fracchiolla, G.; Faliti, S.; Piemontese, L.; Di Giovanni, C.; Iacobazzi, V.; Infantino, V.; Montanari, R.; Capelli, D.; Tortorella, P.; Loiodice, F. New 2-(aryloxy)-3-phenylpropanoic acids as peroxisome proliferator-activated receptor α/γ dual agonists able to upregulate mitochondrial carnitine shuttle system gene expression. *J. Med. Chem.* **2013**, *56*, 60−72.

22. Carbonara, G.; Fracchiolla, G.; Loiodice, F.; Tortorella, P.; Conte-Camerino, D.; De Luca, A.; Liantonio, A. Carboxylic acids and skeletal muscle chloride channel conductance: effects on the biological activity induced by the introduction of an aryloxyalkyl group alpha to the carboxylic function of 4-chloro-phenoxyacetic acid. *Il Farmaco* **2001**, *56*, 749−754.

23. Fracchiolla, G.; Laghezza, A.; Piemontese, L.; Parente, M.; Lavecchia, A.; Pochetti, G.; Montanari, R.; Di Giovanni, C.; Carbonara, G.; Tortorella, P.; Novellino, E.; Loiodice, F. Synthesis, biological evaluation and molecular investigation of fluorinated peroxisome proliferator-activated receptors α/γ dual agonists. *Bioorg. Med. Chem*. **2012**, *20*, 2141−2151.

24. Loiodice, F.; Ferorelli, S.; Tangari, N.; Bettoni, G.; Tortorella, V.; Pierno, S.; De Luca, A.; Tricarico, D.; Conte-Camerino, D. Carboxylic acids and chloride conductance in skeletal muscle: influence on the pharmacological activity induced by the chain substituents and the distance between the phenolic group and the carboxylic function in 4-chloro-phenoxy alkanoic acids. *Il Farmaco* **1993**, *48*, 45−63.

25. Leuci, R.; Brunetti, L.; Laghezza, A.; Piemontese, L.; Carrieri, A.; Pisani, L.; Tortorella, P.; Catto, M.; Loiodice, F. A new series of aryloxyacetic acids endowed with multi-target activity towards peroxisome proliferator-activated receptors (PPARs), fatty acid amide hydrolase (FAAH), and acetylcholinesterase (AChE). *Molecules* **2022**, *27*, 958.

26. Li, S.; Zhu, S.-F.; Xie, J.-H.; Song, S.; Zhang, C.-M.; Zhou. Q.-L. Enantioselective hydrogenation of α-aryloxy and α-alkoxy α,β-unsaturated carboxylic acids catalyzed by chiral spiro iridium/phosphino-oxazoline complexes. *J. Am. Chem. Soc.* **2010**, *132*, 1172–1179.

27. Pinelli, A.; Godio, C.; Laghezza, A.; Mitro, N.; Fracchiolla, G.; Tortorella, V.; Lavecchia, A.; Novellino, E.; Fruchart, J.-C.; Staels, B.; Crestani, M.; Loiodice, F. Synthesis, biological evaluation, and molecular modeling investigation of new chiral fibrates with PPARalpha and PPARgamma agonist activity. *J. Med. Chem.* **2005**, *48*, 5509−5519.

28. Talele, T. T. Opportunities for tapping into three-dimensional chemical space through a quaternary carbon. *J. Med. Chem*. **2020**, *63*, 13291–13315.

29. Muller, K.; Faeh, C.; Diederich, F. Fluorine in pharmaceuticals: looking beyond intuition. *Science* **2007**, *317*, 1881-1886.

30. Hagmann, W. K. The many roles for fluorine in medicinal chemistry. *J. Med. Chem.* **2008**, *51*, 4359-4369.

31. van Marrewijk, L. M.; Polyak, S. W.; Hijnen, M.; Kuruvilla, D.; Chang, M. R.; Shin, Y.; Kamenecka, T. M.; Griffin, P. R.; Bruning. J. B. SR2067 reveals a unique kinetic and structural signature for PPARgamma partial agonism, *ACS Chem. Biol* **2016**, *11*, 273-283.

32. Capelli, D.; Cerchia, C.; Montanari, R.; Loiodice, F.; Tortorella, P.; Laghezza, A.; Cervoni, L.; Pochetti, G.; Lavecchia, A. Structural basis for PPAR partial or full activation revealed by a novel ligand binding mode. *Sci. Rep.* **2016**, *6*, 34792.

33. Hopkins, C. R.; O'Neil, S. V.; Laufersweiler, M. C.; Wang, Y.; Pokross, M.; Mekel, M.; Evdokimov, A.; Walter, R.; Kontoyianni, M.; Petrey, M. E.; Sabatakos, G.; Roesgen, J. T.; Richardson, E.; Demuth, T. P. Jr. Design and synthesis of novel N-sulfonyl-2-indole carboxamides as potent PPAR-γ binding agents with potential application to the treatment of osteoporosis. *Bioorg. Med. Chem. Lett.* **2006**, *16*, 5659−5663.

34. Fujimura, T.; Kimura, C.; Oe, T.; Takata, Y.; Sakuma, H.; Aramori, I.; Mutoh, S. A selective peroxisome proliferator-activated receptor γ modulator with distinct fat cell regulation properties. *J. Pharmacol. Exp. Ther.* **2006**, *318*, 863−871.

35. Lu, I. L.; Huang, C. F.; Peng, Y. H.; Lin, Y. T.; Hsieh, H. P.; Chen, C. T.; Lien, T. W.; Lee, H. J.; Mahindroo, N.; Prakash, E.; Yueh, A.; Chen, H. Y.; Goparaju, C. M.; Chen, X.; Liao, C. C.; Chao, Y. S.; Hsu, J. T.; Wu, S. Y. Structure-based drug design of a novel family of PPARγ partial agonists: virtual screening, X-ray crystallography, and in vitro/in vivo biological activities. *J. Med. Chem*. **2006**, *49*, 2703−2712.

36. Li, Y.; Wang, Z.; Furukawa, N.; Escaron, P.; Weiszmann, J.; lee, G.; Lindstrom, M.; Liu, J.; Xu, H.; Plotnikova, O.; Prasad, V.; Walker, N.; Learned, R. M.; Chen, J. L. T2384, a novel antidiabetic agent with unique peroxisome proliferator-activated receptor γ binding properties. *J. Biol. Chem.* **2008**, *283*, 9168−9176.

37. Motani, A.; Wang, Z.; Weiszmann, J.; McGee, L. R.; Lee, G.; Liu, Q.; Staunton, J.; Fang, Z.; Fuentes, H.; Lindstrom, M.; Liu, J.; Biermann, D. H.; Jaen, J.; Walker, N. P.; Learned, R. M.; Chen, J. L.; Li, Y. INT131: a selective modulator of PPAR gamma. *J. Mol. Biol.* **2009**, *386*, 1301−1311.

38. Sime, M.; Allan, A. C.; Chapman, P.; Fieldhouse, C.; Giblin, G. M. P.; Healy, M. P.; Lambert, M. H.; Leesnitzer, L. M.; Lewis, A.; Merrihew, R. V.; Rutter, R. A.; Sasse, R.; Shearer, B. G.; Wilson, T. M.; Xu, R. X.; Virley, D. J.; Virley, D. J. Discovery of GSK1997132B a novel centrally penetrant benzimidazole PPARγ partial agonist. *Bioorg. Med. Chem. Lett.* **2011**, *21*, 5568−5572.

39. Lillich, F. F.; Willems, S.; Ni, X.; Kilu, W.; Borkowsky, C.; Brodsky, M.; Kramer, J. S.; Brunst, S.; Hernandez-Olmos, V.; Heering, J.; Schierle, S.; Kestner, R. I.; Mayser, F. M.; Helmstädter, M.; Göbel, T.; Weizel, L.; Namgaladze, D.; Kaiser, A.; Steinhilber, D.; Pfeilschifter, W.; Kahnt, A. S.; Proschak, A.; Chaikuad, A.; Knapp, S.; Merk, D.; Proschak, E. Structure-based design of dual partial peroxisome proliferator-activated receptor γ agonists/soluble epoxide hydrolase inhibitors. *J. Med. Chem.* **202**1, *64*, 17259-17276.

40. Ammazzalorso, A.; Bruno, I.; Florio, R.; De Lellis, L.; Laghezza, A.; Cerchia, C.; De Filippis, B.; Fantacuzzi, M.; Giampietro, L.; Maccallini, C.; Tortorella, P.; Veschi, S.; Loiodice, F.; Lavecchia, A.; Cama, A.; Amoroso, R. Sulfonimide and amide derivatives as novel PPARα antagonists: synthesis, antiproliferative activity, and docking studies. *ACS Med. Chem. Lett.* **2020**, *11*, 624-632.

41. Lavecchia, A.; Cerchia, C. Selective PPARγ modulators for type 2 diabetes treatment: how far have we come and what does the future hold? *Future Med. Chem.* **2018**, *10*, 703−705.

42. Laghezza, A.; Piemontese, L.; Cerchia, C.; Montanari, R.; Capelli, D.; Giudici, M.; Crestani, M.; Tortorella, P.; Peiretti, F.; Pochetti, G.; Lavecchia, A.; Loiodice F. Identification of the first PPARα/γ dual agonist able to bind to canonical and alternative sites of PPARγ and to inhibit its Cdk5-mediated phosphorylation. *J. Med. Chem.* **2018**, *61*, 8282–8298.

43. Shang, J.; Kojetin, D. J. Structural mechanism underlying ligand binding and activation of PPARγ. *Structure* **2021**, *29*, 940–950.

44. Pires, D. E.; Blundell, T. L.; Ascher, D. B. pkCSM: predicting small-molecule pharmacokinetic and toxicity properties using graph-based signatures. *J. Med. Chem.* **2015**, *58*, 4066–4072.

45. ACCORD Study Group; Ginsberg, H. N.; Elam, M. B.; Lovato, L. C.; Crouse, J. R., 3rd; Leiter, L. A.; Linz, P.; Friedewald, W. T.; Buse, J. B.; Gerstein, H. C.; Probstfield, J.; Grimm, R. H.; Ismail-Beigi, F.; Bigger, J. T.; Goff, D. C., Jr; Cushman, W. C.; Simons-Morton, D. G.; Byington, R. P. Effects of combination lipid therapy in type 2 diabetes mellitus. *N. Engl. J. Med*. **2010**, *362*, 1563−1574.

46. Guan, Y.; Hao, C.; Cha, D. R.; Rao, R.; Lu, W.; Kohan, D. E.; Magnuson, M. A.; Redha, R.; Zhang, Y.; Breyer, M. D. Thiazolidinediones expand body fluid volume through PPARγ stimulation of ENaC-mediated renal salt absorption. *Nat. Med*. **2005**, *11*, 861−866.

47. Wei, W.; Wang, X.; Yang, M.; Smith, L. C.; Dechow, P. C.; Sonoda, J.; Evans, R. M.; Wan, Y. PGC1α mediates PPARγ activation of osteoclastogenesis and rosiglitazone-induced bone loss. *Cell Metab.* **2010**, *11*, 503−516.

48. Seely, B. L.; Staubs, P. A.; Reichart, D. R.; Berhanu, P.; Milarski, K. L.; Saltiel, A. R.; Kusari, J.; Olefsky, J. M. Protein tyrosine phosphatase 1B interacts with the activated insulin receptor. *Diabetes* **1996**, *45*, 1379–1385.

49. Feldhammer, M.; Uetani, N.; Miranda-Saavedra, D.; Tremblay, M. L. PTP1B: a simple enzyme for a complex world. *Crit. Rev. Biochem. Mol. Biol.* **2013**, *48*, 430–445.

50. Wang, L. J.; Jisng, B.; Wu, N.; Wang, S. Y.; Shi, D. Y. Small molecules as potent protein tyrosine phosphatase 1B (PTP1B) inhibitor documented in patients from 2009 to 2013. *Mini Rev. Med. Chem.* **2015**, *15*, 104–122.

51. Chen, Z.; Vigueira, P. A.; Chambers, K. T.; Hall, A. M.; Mitra, M. S.; Qi, N.; McDonald, W. G.; Colca, J. R.; Kletzien, R. F.; Finck, B. N. Insulin resistance and metabolic derangements in obese mice are ameliorated by a novel peroxisome proliferator-activated receptor γ-sparing thiazolidinedione. *J. Biol. Chem.* **2012**, *287*, 23537–23548.

52. McCommis, K. S.; Hodges, W. T.; Brunt, E. M.; Nalbantoglu, I.; McDonald, W. G.; Holley, C.; Fujiwara, H.; Schaffer, J. E.; Colca, J. R.; Finck, B. N. Targeting the mitochondrial pyruvate carrier attenuates fibrosis in a mouse model of nonalcoholic steatohepatitis. *Hepatology* **2017**, *65*, 1543–1556.

53. Kamm, D. R.; Pyles, K. D.; Sharpe, M. C.; Healy, L. N.; Colca, J. R.; McCommis, K. S. Novel insulin sensitizer MSDC-0602K improves insulinemia and fatty liver disease in mice, alone and in combination with liraglutide. *J. Biol. Chem*. **2021**, *296*, 100807.

54. Divakaruni, A. S.; Wiley, S. E.; Rogers, G. W.; Andreyev, A. Y.; Petrosyan, S.; Loviscach, M.; Wall, E. A.; Yadava, N.; Heuck, A. P.; Ferrick, D. A.; Henry, R. R.; McDonald, W. G.; Colca, J. R.; Simon, M. I.; Ciaraldi, T. P.; Murphy, A. N. Thiazolidinediones are acute, specific inhibitors of the mitochondrial pyruvate carrier. *Proc. Natl. Acad. Sci. U. S. A.* **2013**, *110*, 5422–5427.

55. Hodges, W. T.; Jarasvaraparn, C.; Ferguson, D.; Griffett, K.; Gill, L. E.; Chen, Y.; Ilagan, M. X. G.; Hegazy, L.; Elgendy, B.; Cho, K.; Patti, G. J.; McCommis, K. S.; Finck, B. N. Mitochondrial pyruvate carrier inhibitors improve metabolic parameters in diet-induced obese mice. *J. Biol. Chem.* **2022**, *298*, 101554.

56. Zangari, J.; Petrelli, F.; Maillot, B.; Martinou, J. C. The multifaceted pyruvate metabolism: role of the mitochondrial pyruvate carrier. *Biomolecules* **2020**, *10*, 1068.

57. Veliova, M.; Ferreira, C. M.; Benador, I. Y.; Jones, A. E.; Mahdaviani, K.; Brownstein, A. J.; Desousa, B. R.; Acín-Pérez, R.; Petcherski, A.; Assali, E. A.; Stiles, L.; Divakaruni, A. S.; Prentki, M.; Corkey, B. E.; Liesa, M.; Oliveira, M. F.; Shirihai, O. S. Blocking mitochondrial pyruvate import in brown adipocytes induces energy wasting via lipid cycling. *EMBO Rep.* **2020**, *21*, e49634.

58. McCommis, K. S.; Chen, Z.; Fu, X.; McDonald, W. G.; Colca, J. R.; Kletzien, R. F.; Burgess, S. C.; Finck, B. N. Loss of mitochondrial pyruvate carrier 2 in the liver leads to defects in gluconeogenesis and compensation via pyruvate-alanine cycling. *Cell Metab.* **2015**, *22*, 682–694.

59. Divakaruni, A. S.; Wallace, M.; Buren, C.; Martyniuk, K.; Andreyev, A. Y.; Li, E.; Fields, J. A.; Cordes, T.; Reynolds, I. J.; Bloodgood, B. L.; Raymond, L. A.; Metallo, C. M.; Murphy, A. N.

Inhibition of the mitochondrial pyruvate carrier protects from excitotoxic neuronal death. *J. Cell Biol.* **2017**, *216*, 1091–1105.

60. Charton, J.; Gauriot, M.; Totobenazara, J.; Hennuyer, N.; Dumont, J.; Bosc, D.; Marechal, X.; Elbakali, J.; Herledan, A.; Wen, X.; Ronco, C.; Gras-Masse, H.; Heninot, A.; Pottiez, V.; Landry, V.; Staels, B.; Liang, W. G.; Leroux, F.; Tang, W. J.; Deprez, B.; Deprez-Poulain, R. Structure-activity relationships of imidazole-derived 2-[N-carbamoylmethyl-alkylamino]acetic acids, dual binders of human insulin-degrading enzyme. *Eur. J. Med. Chem.* **2015**, *90*, 547–567.

61. Friesner, R. A.; Banks, J. L.; Murphy, R. B.; Halgren, T. A.; Klicic, J. J.; Mainz, D. T.; Repasky, M. P.; Knoll, E. H.; Shelley, M.; Perry, J. K.; Shaw, D. E.; Francis, P.; Shenkin, P. S. Glide: a new approach for rapid, accurate docking and scoring. 1. Method and assessment of docking accuracy. *J. Med. Chem.* **2004**, *47*, 1739–1749.

62. Halgren, T. A.; Murphy, R. B.; Friesner, R. A.; Beard, H. S.; Frye, L. L.; Pollard, W. T.; Banks, J. L. Glide: a new approach for rapid, accurate docking and scoring. 2. Enrichment factors in database screening. *J. Med. Chem.* **2004**, *47*, 1750–1759.

63. Hollon, T.; Yoshimura, F.K. Variation in enzymatic transient gene expression assays. *Anal. Biochem.* **1989**, *182*, 411–418.

64. Yasmin, S.; Capone, F.; Laghezza, A.; Piaz, F. D.; Loiodice, F.; Vijayan, V.; Devadasan, V.; Mondal, S. K.; Atlı, Ö.; Baysal, M.; Pattnaik, A. K.; Jayaprakash, V.; Lavecchia, A. Novel benzylidene thiazolidinedione derivatives as partial PPARγ Agonists and their antidiabetic effects on type 2 diabetes. *Sci. Rep*. **2017**, *7*, 14453.

65. Ottanà, R.; Paoli, P.; Lori, G.; Adornato, I.; Previti, S.; Naß, A.; Wolber, G.; Maccari, R. Design and evaluation of non-carboxylate 5-arylidene-2-thioxo-4-imidazolidinones as novel non-competitive inhibitors of protein tyrosine phosphatase 1B. *Bioorg. Chem*. **2019**, *92*, 103211.

66. Ottanà, R.; Paoli, P.; Cappiello, M.; Nguyen, T. N.; Adornato, I.; Del Corso, A.; Genovese, M.; Nesi, I.; Moschini, R.; Naß, A.; Wolber, G.; Maccari, R. In search for multi-target ligands as potential agents for diabetes mellitus and its complications-A structure-activity relationship study on inhibitors of aldose reductase and protein tyrosine phosphatase 1B. *Molecules* **2021**, *26*, 330.

67. Sblano, S.; Cerchia, C.; Laghezza, A.; Piemontese, L.; Brunetti, L.; Leuci, R.; Gilardi, F.; Thomas, A.; Genovese, M.; Santi, A.; Tortorella, P.; Paoli, P.; Lavecchia, A.; Loiodice F. A chemoinformatics search for peroxisome proliferator-activated receptors ligands revealed a new pan-agonist able to reduce lipid accumulation and improve insulin sensitivity. *Eur. J. Med. Chem*. **2022**, *235*, 114240.

68. Pranzini, E.; Pardella, E.; Muccillo, L.; Leo, A.; Nesi, I.; Santi, A.; Parri, M.; Zhang, T.; Uribe, A. H.; Lottini, T.; Sabatino, L.; Caselli, A.; Arcangeli, A.; Raugei, G.; Colantuoni, V.; Cirri, P.; Chiarugi, P.; Maddocks, O.; Paoli, P.; Taddei, M. L. SHMT2-mediated mitochondrial serine metabolism drives 5-FU resistance by fueling nucleotide biosynthesis. *Cell reports* **2022**, *40*, 111233.

Table of Contents graphic